Molecular Therapy
Original Article

Transplantation of dorsal root ganglia overexpressing the NaChBac sodium channel improves locomotion after complete SCI

Sonia Hingorani,[1] Guillem Paniagua Soriano,[1] Carlos Sánchez Huertas,[2] Eva María Villalba Riquelme,[3] Eric López Mocholi,[1] Beatriz Martínez Rojas,[1] Ana Alastrué Agudo,[1] Sebastián Dupraz,[4] Antonio Vicente Ferrer Montiel,[3] and Victoria Moreno Manzano[1]

[1]Neuronal and Tissue Regeneration Laboratory, Centro de Investigación Príncipe Felipe, 46012 Valencia, Spain; [2]Development and Assembly of Bilateral Neural Circuits Laboratory, Instituto de Neurociencias, Consejo Superior de Investigaciones Científicas (CSIC)-Universidad Miguel Hernández, Avenida Santiago Ramon y Cajal, s/n, 03550 Sant Joan d'Alacant, Alicante, Spain; [3]Biochemistry and Molecular Biology Department, Instituto de Investigación, Desarrollo e Innovación en Biotecnología Sanitaria de Elche-IDiBE, Avenida de la Universidad, s/n, Edificio Torregaitán, 03202 Elche, Alicante, Spain; [4]Laboratory for Axonal Growth and Regeneration, German Center for Neurodegenerative Diseases (DZNE), 53127 Bonn, Germany

Spinal cord injury (SCI) is a debilitating condition currently lacking treatment. Severe SCI causes the loss of most supraspinal inputs and neuronal activity caudal to the injury, which, coupled with the limited endogenous capacity for spontaneous regeneration, can lead to complete functional loss even in anatomically incomplete lesions. We hypothesized that transplantation of mature dorsal root ganglia (DRGs) genetically modified to express the NaChBac sodium channel could serve as a therapeutic option for functionally complete SCI. We found that NaChBac expression increased the intrinsic excitability of DRG neurons and promoted cell survival and neurotrophic factor secretion *in vitro*. Transplantation of NaChBac-expressing dissociated DRGs improved voluntary locomotion 7 weeks after injury compared to control groups. Animals transplanted with NaChBac-expressing DRGs also possessed higher tubulin-positive neuronal fiber and myelin preservation, although serotonergic descending fibers remained unaffected. We observed early preservation of the corticospinal tract 14 days after injury and transplantation, which was lost 7 weeks after injury. Nevertheless, transplantation of NaChBac-expressing DRGs increased the neuronal excitatory input by an increased number of VGLUT2 contacts immediately caudal to the injury. Our work suggests that the transplantation of NaChBac-expressing dissociated DRGs can rescue significant motor function, retaining an excitatory neuronal relay activity immediately caudal to injury.

INTRODUCTION

Severe spinal cord injury (SCI) is a devastating life-altering condition lacking cure. Multiple concomitant inhibitory factors accumulate after injury,[1,2] but the main long-term obstacles include lack of intrinsic axonal regeneration[3] and loss of adequate activity in spared tissue in the absence of supraspinal inputs.[4] Nevertheless, patients with incomplete injuries can recover motor function due to spontaneous neuroplasticity and reactivation of spared dormant connections.[5,6] Enhancing spontaneous sprouting, forming relay circuits within spare axons, and activating dormant circuits after injury constitute strategies that promote significant functional recovery. In rodents and primates, spontaneous improved locomotor function may derive from increased sprouting of descending tracts,[7–10] including the corticospinal tract (CST)[9,11] and the reticulospinal tract,[12] and formation of relay circuits by propriospinal interneurons.[13] These processes can be enhanced by electrical stimulation,[14] direct genetic manipulation of the CST by co-deletion of *PTEN* and *SOCS3*,[15] creation of a permissive environment by chondroitinase release,[10] or pharmacological treatments targeting dormant relays.[5] Studies reveal injury-induced synaptic-input alterations in motor neurons caudal to the injury, including a decrease in excitatory input,[16] and neurotransmitter switch in spinal interneurons resulting in alteration of the excitation/inhibition ratio,[17] explaining relay circuit latency, dysfunction of motor neurons, and limited recovery.[16,17] Therefore, enhancing the excitatory input from long descending projections (supraspinal and propriospinal neurons[13]) and reducing the inhibitory input from local interneuron circuits[5,18] could restore activity across the lesion.

Cell therapies,[19] particularly neural stem and progenitor cell transplantation,[8,20] are considered promising therapy for SCI, aiming to induce functional recovery by restoring neuronal circuits.[21] However, reported disadvantages of neural stem cell transplantation include limited capacity to integrate within endogenous neuronal circuits, reduced survival in the harmful injury environment,[22] and diminished ability to generate mature neurons.[23]

Received 6 December 2023; accepted 28 March 2024;
https://doi.org/10.1016/j.ymthe.2024.03.038.

Correspondence: Victoria Moreno Manzano, Centro de Investigación Príncipe Felipe, Eduardo Primo de Yúfera 3, 46012 Valencia, Spain.
E-mail: vmorenom@cipf.es

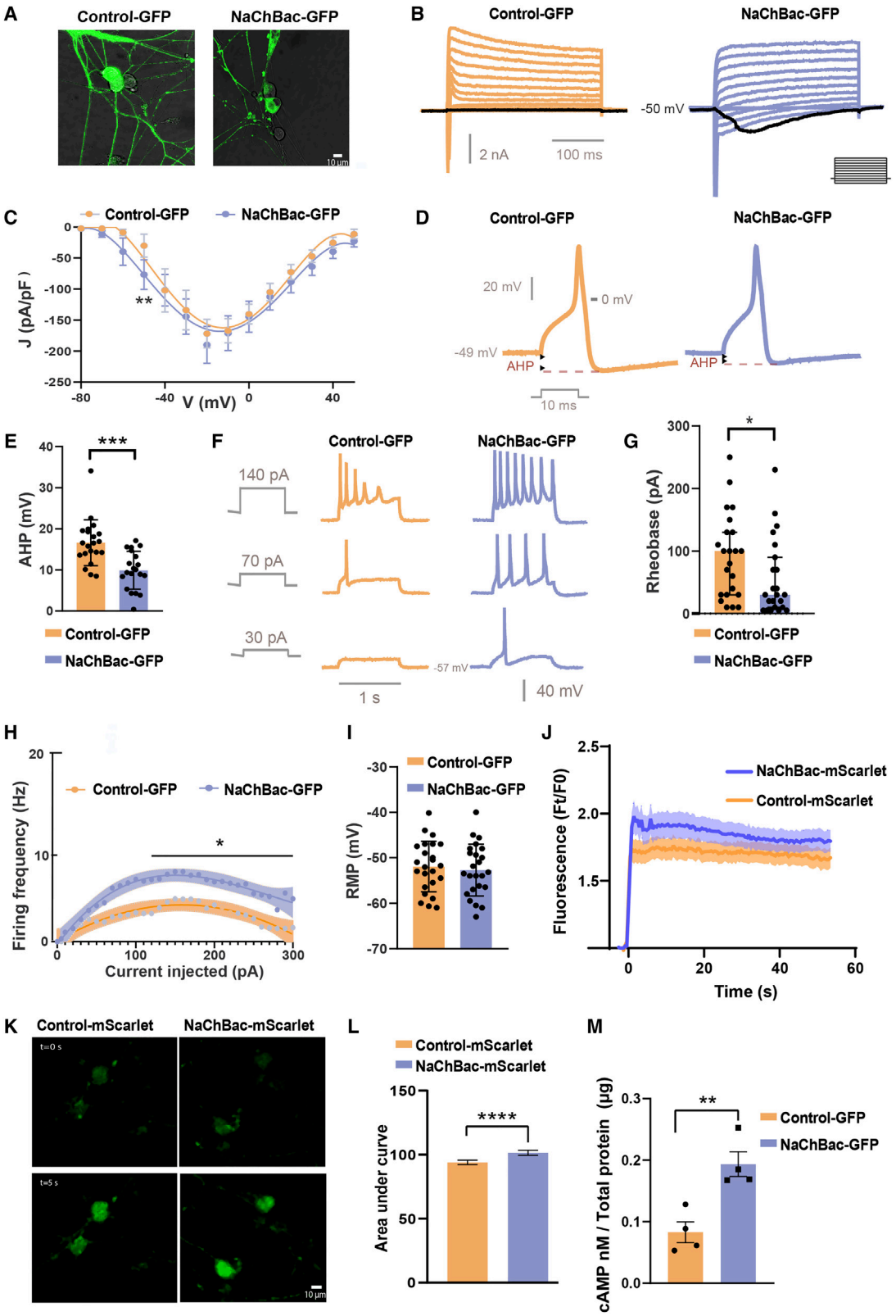

(legend on next page)

Although not used extensively for SCI treatment, transplantation of mature central nervous system (CNS) neurons has successfully restored lost connections in brain injuries and diseases.[24–26] Alternatively, peripheral nervous tissue use has been extensive[27] due to its elevated regenerative capacity. Isolated dorsal root ganglion (DRG) neurons can survive, extend, and integrate to form new connections within the spinal cord.[28–30] Minimally invasive transplants of postnatal or adult DRGs into the injured brain prompt the projection of contralateral long axons and robust integration into the white matter of the adult rat brain.[31] In the adult rat spinal cord, adult DRG neurons survived and extended up to 5 mm when microtransplanted distal to a primary trauma; but were unable to cross the inhibitory scar, limiting their ability to contribute to the reactivation of denervated circuits caudal to the lesion.[32]

Given the activity-dependent nature of neuronal survival and integration into circuits,[33–35] manipulation of neuronal activity has been exploited for SCI treatment. The ectopic expression of a bacterial sodium voltage-gated ionic channel (NaChBac) modulated intrinsic neuronal activity by decreasing the firing threshold.[36] Furthermore, NaChBac expression decreased apoptosis and increased the survival of newly formed olfactory neurons[37] and cortical interneurons[38] and increased neuronal integration into existing circuits.[37–39]

We hypothesized that transplantation of NaChBac-expressing dissociated DRGs could enhance their inherent integrative and survival capacities, helping overcome the inhibitory environment to treat SCI. Indeed, transplantation of NaChBac-expressing dissociated DRGs rescues significant motor function and retains an excitatory neuronal relay activity immediately caudal to injury.

RESULTS

NaChBac expression increases the excitability of neonatal rat DRG neurons

Expression of NaChBac fused to GFP in rat neonatal DRG neurons was located at the cytosolic membrane (Figure 1A) and modulated DRG activity characterized by intracellular electrophysiological recordings (Figures 1B–1I). Single-cell patch-clamp recordings of NaChBac-GFP DRG neurons revealed a slow inward current at −50 mV, absent in Control-GFP DRG neurons (Figures 1B and 1C). We observed a modified action potential waveform in NaChBac-GFP DRG neurons (Figure 1D), resulting in a significantly smaller after-hyperpolarization (AHP) phase compared to Control-GFP DRG neurons (Figure 1E). These alterations induced modified action potential firing in NaChBac-GFP DRG neurons (Figure 1F), a decrease in the rheobase (Figure 1G), and a significant increase in the firing frequency (in Hz) (Figure 1H). NaChBac-GFP did not alter the resting membrane potential (Figure 1I) or input resistance (Table S1), as noted previously.[40,41]

Since NaChBac expression elevates spontaneous calcium (Ca^{2+} currents in developing cortical neurons,[41] we performed real-time imaging of Ca^{2+} dynamics using Fluo-4AM conjugated with Alexa 488 in NaChBac-mScarlet or Control-mScarlet DRG neurons. When depolarized with KCl, NaChBac-mScarlet neurons displayed higher Ca^{2+} signaling, which persisted for at least 60 s (Figures 1J–1L). Given that Ca^{2+} signaling modulates adenyl cyclases and cAMP generation,[42] we found an increase in cAMP levels detected by chromatography in NaChBac-GFP dissociated DRGs compared to Control-GFP dissociated DRGs (Figure 1M).

These findings provide evidence that NaChBac-GFP expression in DRG neurons leads to higher intrinsic excitability, which leads to an increased influx of intracellular Ca^{2+} and elevated cAMP levels.

NaChBac expression enhances cell survival, pro-survival signaling in murine neuroblastoma cells, and increased neurotrophic factor secretion

We evaluated the effect of NaChBac induced expression on cell survival using the neuroblastoma line Neuro-2A (N2A), given their wide use to study several neuronal pathways due to their ability to proliferate and differentiate into neurons.[43] Stable expression was achieved by lentiviral transduction. We found NaChBac-GFP expression restricted to the cell membrane, but the GFP expression pattern was uniform and cytoplasmic for Control-GFP (Figure 2A), as shown in Figure 1A. Cell proliferation analysis revealed that NaChBac-GFP significantly increased the number of N2A cells after 4 and 5 days in culture before reaching confluency (Figure 2B). In addition, NaChBac-GFP expression prevented N2A cell death after exposure to hypoxia (1% oxygen) for 24 h (Figure 2C).

To study cell survival signaling pathways, we assessed active phosphorylation levels (p) of AKT and mTOR proteins[40,44] and total levels

Figure 1. NaChBac expression impact on rat neonatal DRG neurons

(A) DRG neurons expressing Control-GFP or NaChBac-GFP 72 h after lentiviral transduction. Scale bar, 10 μm (B) Family of current traces evoked by a 300 ms voltage step protocol from −80 to 50 mV in 10 mV increments in Control-GFP and NaChBac-GFP DRG neurons. Holding potential, −60 mV. Black trace displays current elicited at −50 mV. (C) Current density-voltage (J-V) relationships were obtained with the protocol described in (F). $^{**}p = 0.0025$, Mann-Whitney test. (D) Representative action potentials recorded in Control-GFP and NaChBac-GFP DRG neurons. Action potentials were evoked with a 10 ms depolarizing current pulse. (E) Amplitude of the AHP in neurons. $^{***}p = 0.0002$, Mann-Whitney test. (F) Representative action potential firing evoked by 1 s depolarizing current pulses for Control-GFP and NaChBac-GFP DRG neurons. (G) Rheobase for eliciting action potential in Control-GFP and NaChBac-GFP DRG neurons. $^{*}p = 0.0302$, Mann-Whitney test. (H) Action potential firing induced by increasing 1 s current pulses (0–300 pA), as shown in (F). Mann-Whitney test, $^{*}p < 0.005$. (I) Resting membrane potential for Control-GFP and NaChBac-GFP DRG neurons. For electrophysiology experiments, each dot represents a neuron; $n = 25–30$, 3 independent experiments. (J) Graph showing change in Ca^{2+} as measured by the difference in fluorescence intensity of Fluo-4AM after adding 100 mM KCl to the culture throughout imaging time frame (60 s). (K) Representative images of Control-mScarlet and NaChBac-mScarlet DRG neurons at t = 0 s (before the addition of KCl) and t = 5 s after the addition of 100 mM KCl, previously treated with Fluo-4AM (green). Scale bar, 10 μm. (L) Area under the curve of (J). Unpaired t test, $^{****}p < 0.0001$, $n = 3$. (M) cAMP quantification normalized to total protein content in Control-GFP and NaChBac-GFP dissociated DRGs, $n = 4$, $^{**}p = 0.0056$, unpaired Student's t test. Data presented as mean ± SEM, $n = 3$ (unless specified).

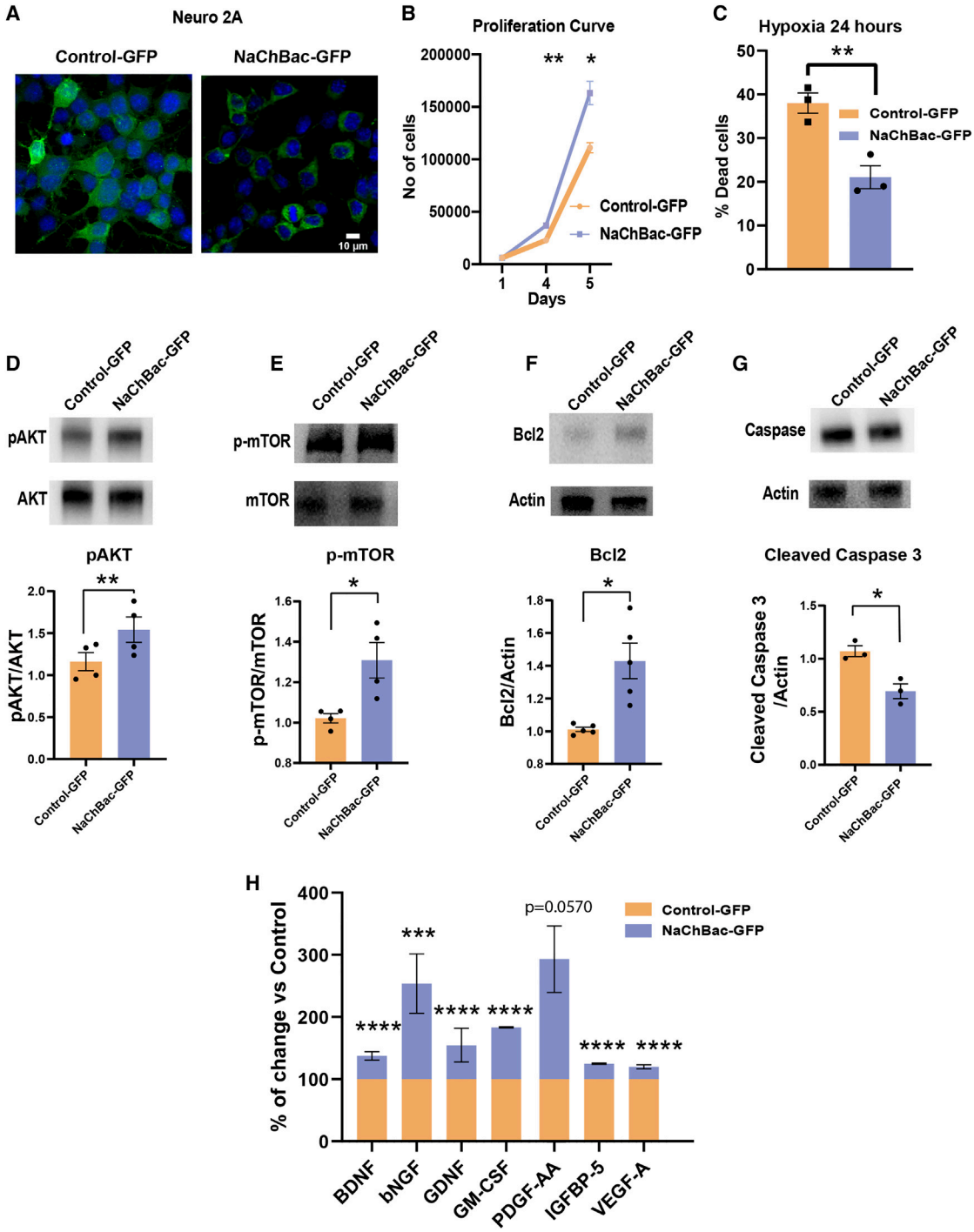

Figure 2. NaChBac expression enhances neuroblastoma cell survival signaling and increases secretion of neurotrophic factors in DRG cultures

(A) Representative images of N2A cells expressing Control-GFP (left, green) or NaChBac-GFP (right, green). Cell nuclei were stained with DAPI (blue); scale bar, 10 µm. (B) Proliferation curve for Control-GFP and NaChBac-GFP N2A cells, absolute number of cells counted; $n = 3$. $^{**}p = 0.0038$, day 4; $^{*}p = 0.013$, day 5, unpaired t test. (C) Percentage of N2A cell death after 24 h of hypoxia (1% O_2); $n = 3$; $^{**}p = 0.0082$, unpaired t test. (D–G) Representative western blots (top) and semiquantitative analysis (bottom) of (D) p-AKT (normalized to total AKT protein levels), $^{**}p = 0.001$, $n = 3$; (E) p-mTOR protein (normalized to total mTOR protein levels), $^{*}p = 0.01$, $n = 4$; (F) Bcl2 protein (normalized to actin), $^{*}p = 0.01$, $n = 5$; and (G) cleaved caspase 3 (normalized to actin), $^{*}p = 0.04$, $n = 3$. Ratio paired t test; two-tailed. (H) Graph showing the increase in the levels of neurotrophic factors of NaChBac-GFP compared to Control-GFP after quantification of array. Multiple unpaired t test, BDNF $^{****}p < 0.000001$; bNGF $^{***}p = 0.0082$; GDNF $^{****}p = 0.000727$; GM-CSF $^{****}p < 0.000001$; PDGF-AA $p = 0.057$; IGFBP-5 $^{****}p = 0.000002$; VEGF-A $^{****}p = 0.000226$. Data presented as mean ± SEM.

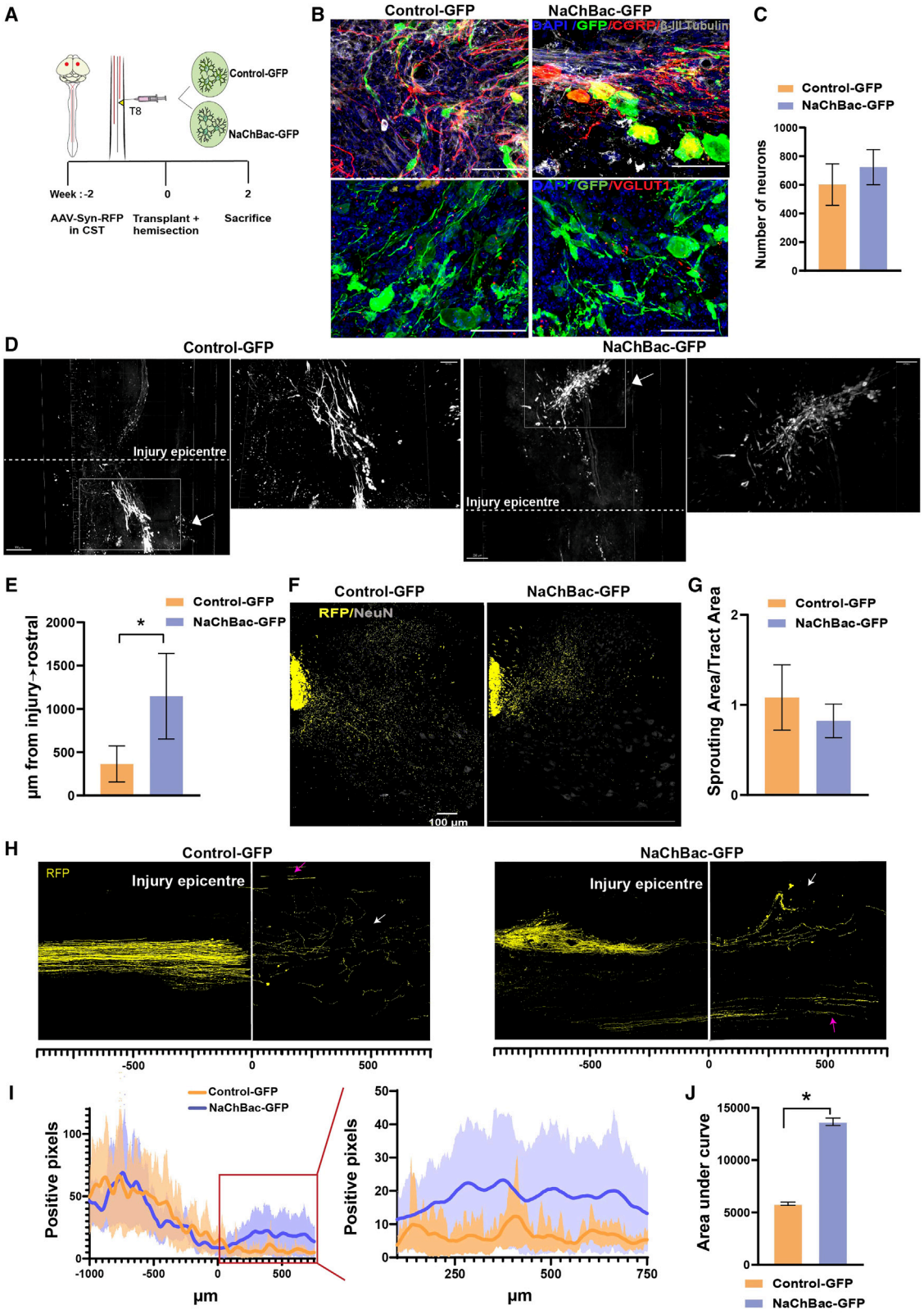

(legend on next page)

of Bcl2 and caspase 3 proteins.[45,46] NaChBac-GFP expression led to an increase in the active forms of AKT (p-AKT, Figure 2D) and mTOR (p-mTOR, Figure 2E) and in total levels of the antiapoptotic Bcl2 protein (Figure 2F). Conversely, NaChBac-GFP expression reduced the levels of the cleaved caspase 3, a pro-apoptotic marker (Figure 2G). Our findings reveal that NaChBac expression increases N2A proliferation, prevents hypoxia-induced cell death, and increases cell-survival-related signaling. Next, we evaluated the mechanism of action of NaChBac expression-induced changes in DRGs. Since cAMP or Ca^{2+}-dependent signaling can increase the expression and secretion of pro-survival factors such as brain-derived neurotrophic factor (BDNF),[47] vascular endothelial growth factor (VEGF),[48] or glial-derived neurotrophic factor (GDNF),[49] we performed a multiarray, containing up to 14 different growth factors, using the media obtained from Control-GFP or NaChBac-GFP mixed DRG cultures. We found a significant release of BDNF, GDNF, nerve growth factor (NGF), granulocyte macrophage colony-stimulating factor (GM-CSF), insulin-like growth factor 1 (IGF-1), platelet-derived growth factor (PDGF) isoform AA, insulin-like growth factor binding protein 5 (IGFBP5), and VEGF (Figure 2H).

Transplantation of NaChBac-expressing DRG neurons increases CST preservation in a mouse model of SCI by single lateral hemisection

NaChBac expression enhanced the survival of newly formed migrating neurons with increased integration into existing circuits.[39] Hence, we hypothesized that NaChBac expression could alter the survival and/or integration of transplanted DRG neurons. DRGs from neonate rats, P3–P4 (Figure 1A), were transduced with pLL3.7 empty vector (Control-GFP) or pLL3.7-NaChBac-eGFP (NaChBac-GFP) and cultured for 5 days prior to transplantation into adult mice immediately below a lateral hemisection at the eighth thoracic vertebra level (T8). Despite treatment with cytosine arabinoside (AraC) to avoid glial proliferation, the presence of glia was not completely excluded (Figure S1A). CST was traced by injecting AAV-Syn-RFP into the motor cortex 2 weeks before the injury, and transplantation was performed, as described in Hilton et al.[50] Two weeks later, animals were sacrificed to assess localization, survival, and integration of Control-GFP and NaChBac-GFP DRG neurons (Figure 3A, experimental design).

Transplanted DRG neurons, characterized by a large soma and long neurites (Figure S1D), some of which were positive for calcitonin gene-related peptide (CGRP) expression[51,52] (Figure 3B, red), were found at the injury site (Figures 3B and S1B). However, we did not observe significant differences in the number of neurons between mice transplanted with Control-GFP and NaChBac-GFP DRG neurons (Figure 3C); rather, we counted a higher total number of GFP-positive cells (neurons and glial cells) in NaChBac-GFP mice than in Control-GFP mice (Figures S1B and S1C).

Transplanted NaChBac-GFP DRG neurons migrated longer distances from the injection site to rostral locations surrounding the descending CST than Control-GFP DRG neurons (Figures 3D and 3E, clarified spinal cord images). Previous reports show increased migratory and integration capacity in developing neurons in the olfactory system after NaChBac expression.[39] Since endogenous Ca^{2+} and neuronal activity play essential roles in neuronal migration,[53] an increase in the endogenous activity of NaChBac-GFP neurons may be associated with increased migratory capacity. Transplantation at earlier time points correlates with a rostral migratory phenotype, possibly due to the presence of an inhibitory inflammatory environment at the injury site during the initial stages.[54]

The CST is the central tract involved in skilled voluntary motor functions.[7,55] CST sprouting after injury has been linked to improved neural activity[56,57] and enhanced functional recovery.[9,11] Since transplanted NaChBac-GFP DRG neurons migrated closer to the injured CST rostral projection (Figure 3D), we analyzed whether these could enhance rostral CST sprouting of injured axons. However, this did not have any effect on CST sprouting after transplantation in Control-GFP and NaChBac-GFP mice (Figures 3F and 3G). Nevertheless, we found an increase in the amount of red fluorescent protein (RFP)-expressing CST fibers preserved at the injury site in the NaChBac-GFP transplanted group (Figure 3H, yellow), measured as RFP-positive pixels extending up to 750 μm after the injury epicenter (marked as 0 in Figure 3I), in comparison to Control-GFP DRG-neuron-transplanted mice (Figure 3J). Of note, we observed a higher tendency of CST axons to cross DRG-NaChBac grafts rather than Control-GFP grafts ($p = 0.1$), suggesting that NaChBac-GFP DRG cells provide a substrate for CST preservation (Figures S2A and S2B).

Overall, NaChBac expression in DRGs enhances migratory activity and contributes partially to preserving the CST projection at the injury epicenter, without altering the survival of transplanted DRG neurons 2 weeks after transplantation.

Figure 3. Transplanted NaChBac-expressing DRG neurons display improved migration and CST preservation ability

(A) Experimental timeline depiction. (B) Representative confocal images of Control-DRG (left) or NaChBac-GFP (right) showing DRG neurons (green), fibers and DRG neurons positive for CGRP (red), and VGLUT1 vesicles (red). All nuclei are stained with DAPI (blue). Scale bars, 100 μm. (C) Neuronal survival measured 2 weeks after transplantation; $n = 4$, unpaired Student' s t test. (D) Clear, Unobstructed Brain Imaging cocktails and Computational analysis (CUBIC)-clarified whole spinal cord-derived images of mice after Control-GFP and NaChBac-GFP DRG transplantation; gray, GFP; arrow, injury epicenter. Scale bars, 200 μm. White boxes mark amplified images. Scale bars, 50 μm. (E) Cell migration 2 weeks after transplantation of Control-GFP and NaChBac-GFP DRG neurons; $n = 7–8$; $^*p = 0.050$, Mann-Whitney test. (F) Representative images of CST sprouting rostral to the lesion in transplanted mice. Yellow, RFP (traced CST); gray, NeuN (neurons). Scale bar, 100 μm. (G) Quantification of sprouting area normalized to tract area; $n = 7–8$, unpaired Student's t test. (H) Representative RFP-expressing CST fiber (yellow) preservation images after T8 lateral hemisection 2 weeks after transplant. Pink arrows point uninjured CST fibers; white arrows point injured CST. (I) Quantification of positive RFP-expressing CST pixels (yellow) before and after the injury epicenter (white line marked in 3H) in Control-GFP and NaChBac-GFP DRG-neuron-transplanted mice. (J) Area under the curve for CST crossing the injury epicenter up to 750 μm, from (I); $n = 8–9$; $^*p = 0.02$, unpaired t test. Data presented as mean ± SEM.

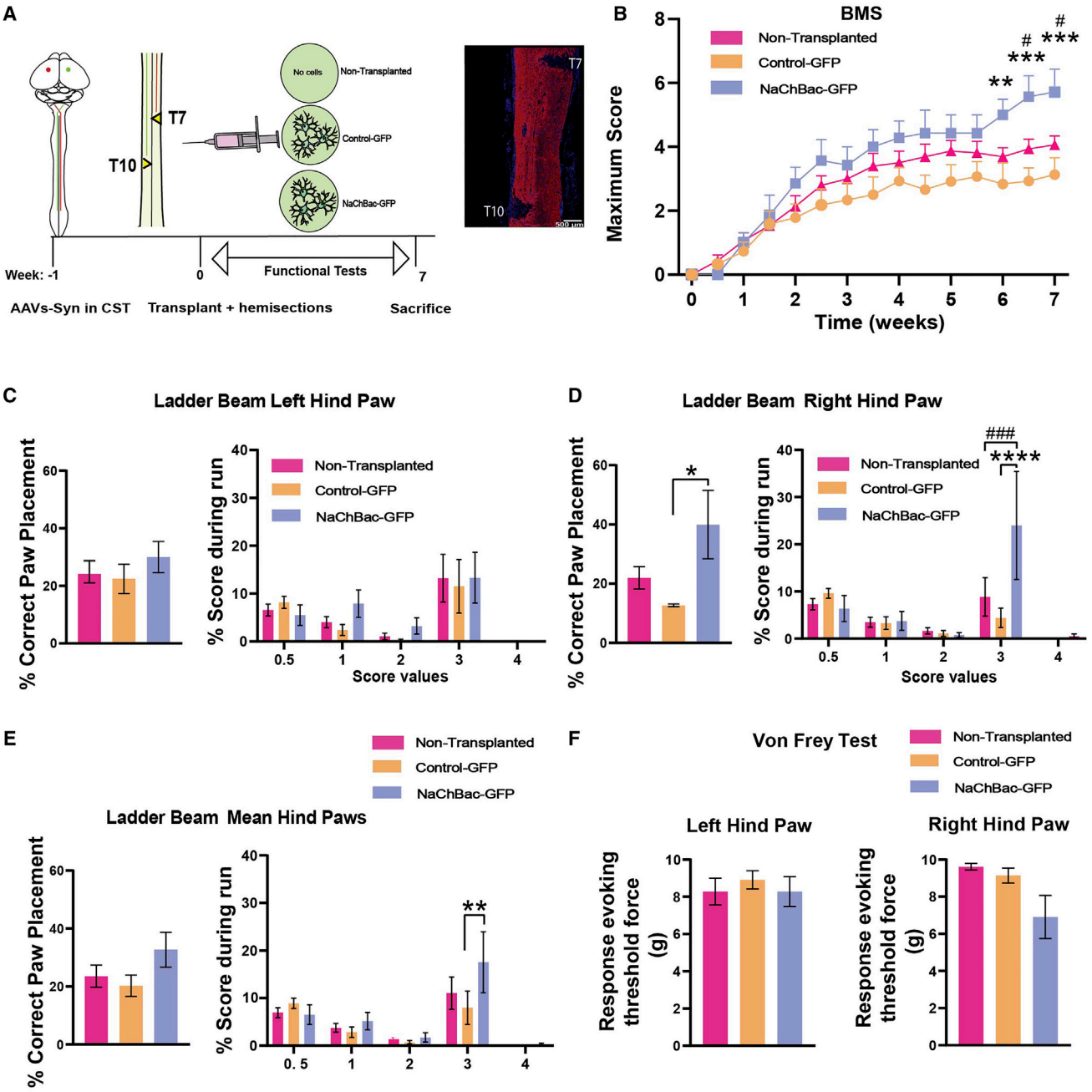

Figure 4. Evaluation of functional recovery 7 weeks after transplantation of NaChBac-expressing DRG neurons

(A) Schematic description of experimental timeline. Mice were traced with AAV-Syn-GFP or -RFP, followed by a double lateral hemisection at T7 and T10 and immediately transplanted with NaChBac-GFP transplant, Control-GFP transplant, or equivalent medium (non-transplanted). Scale bar 500 μm. (B) BMS graph depicting scores throughout the experimental time frame in all treatment groups. Two-way ANOVA followed by Tukey's *post hoc* test, $n = 7–15$. Week 6, Control-GFP vs. NaChBac-GFP, $^{**}p = 0.004$; weeks 6.5 and 7, Control-GFP vs. NaChBac-GFP, $^{***}p = 0.0002$; and non-transplanted vs. NaChBac-GFP, $^{\#}p = 0.03$. (C) Graphs depicting the percentage correct left-hindpaw placement of animals from all treatment groups in the ladder beam test 1 day before sacrifice (left), and the percentage of animals from each treatment group receiving the scores for the ladder beam test (right). (D) Graphs depicting the percentage of correct right-hindpaw placement of animals from all treatment groups in the ladder beam test 1 day before sacrifice (left), and the percentage of animals from each treatment group receiving the scores for the ladder beam test (right). Left, one-way ANOVA followed by Tukey's *post hoc* test, $^{*}p = 0.03$. Right, two-way ANOVA followed by Tukey's *post hoc* test, non-transplanted vs. NaChBac-GFP, $^{\#\#\#}p = 0.0002$; Control-GFP vs.

(legend continued on next page)

Transplanted NaChBac-expressing DRG transplants improve locomotor function after complete SCI in a double-staggered hemisection model

We next asked whether transplantation of NaChBac-expressing dissociated DRGs could improve connectivity, CST preservation, and functional outcome in a severe, chronic SCI model. For this, we performed two lateral thoracic hemisections (right, T7, and left, T10; Figure 4A), ensuring the ablation of all descending pathways after the T10 lateral hemisection.[58] This allows the evaluation of the pro-regenerative capacity of grafts of DRGs expressing NaChBac-GFP (NaChBac-GFP) when transplanted between hemisections compared to dissociated DRGs expressing Control-GFP (Control-GFP) and non-transplanted animals (non-transplanted).

We traced the CST 1 week before injury (and transplantation) in all animals by injecting AAV-Syn-GFP into the right hemisphere and AAV-Syn-RFP into the left hemisphere of the motor cortex[50] (Figure 4A). Functional evaluation using open-field locomotor assessment using the Basso mouse scale (BMS) score[59] of all three treatment groups (non-transplanted and Control-GFP and NaChBac-GFP DRG transplants) revealed a steady improvement in the locomotor function of NaChBac-GFP-DRG-transplanted mice, with significant improvements compared to the Control-GFP-DRG-transplanted and non-transplanted mice 7 weeks after injury and transplantation (Figure 4B).

We performed a horizontal ladder beam test to evaluate the locomotion of each hindlimb separately.[60] We did not observe any significant differences in the percentage of correct paw placement in the left hindlimb (T10 hemisection) between the treatment groups (Figure 4C, left) nor in the percentage of animals reaching each score point (Figure 4C, right). However, we did observe a significant increase in the percentage of correct paw placement in the right hindlimb (T7 hemisection) in NaChBac-GFP mice compared to Control-GFP mice (Figure 4D, left) and in the percentage of mice reaching a score of 3 in the NaChBac-GFP-DRG-transplanted group compared to both control groups (Figure 4D, right). When analyzing the percentage of correct paw placement for the mean of hindlimbs (Figure 4F, left), we found a significant increase in the percentage of animals reaching score point 3 in NaChBac-GFP mice compared to Control-GFP mice (Figure 4E, right). Score 3 of the ladder beam corresponds to toe step and reveals whether mice can support weight and exhibit improved coordination.[60] Finally, although DRG neuron excitability has been related to nociception, the Von Frey filament test of allodynia revealed that transplantation does not induce significant differences in the response-evoking force (g) (Figure 4F).

Overall, mice receiving NaChBac-GFP transplant exhibited improved locomotor function without altering nociception compared to Control-GFP and non-transplanted mice.

Transplanted NaChBac-expressing dissociated DRGs enhance neuronal fiber preservation rostral to the injury site but not CST or serotonergic tract preservation

To identify the mechanisms behind the functional improvement in NaChBac-GFP transplanted mice, we performed histological analysis. We evaluated the injured area (negative for GFAP staining) as previously described,[61] including the T7 and T10 opposite hemisections (Figure 5A, yellow line delimits the GFAP-negative area). We did not find significant differences in the total injury area between treatment groups, ensuring the homogeneity of the injuries (Figure 5B). In addition, we studied the astrocytic reactivity by measuring the GFAP staining intensity of the astrocytes delimiting the injury border (Figure S3A, left, dotted lines), but did not observe any differences between the groups (Figure S3A, right) nor in the fibronectin staining found within the injury (Figure S3B). Of note, we also studied the effect of NaChBac expression on the immunological profile of the injuries, in both models, after single lateral hemisection (Figure S3D) and after double-staggered hemisection model (Figure S3C), by Iba-1 staining, including microglia and infiltrated macrophages, within the injury site. We found no significant differences in the percentage of reactive (circular) Iba-1-positive cells within the groups in any of the evaluated models (Figures S3C and S3D).

Increased sprouting from descending tracts may improve relay circuit activity by innervating propriospinal interneurons in double-staggered hemisection models.[5,13] Therefore, we asked whether NaChBac-GFP transplant could increase the CST preservation or sprouting between hemisections at the injury site (Figures 5C–5E). However, like previous CST sprouting analysis (Figure 3), we did not find differences in the sprouting area of CST axons (Figure 5C). Mice from all groups displayed complete degeneration after the first hemisection of descending CST labeled with AAV-hSyn-GFP (Figure 5D, white arrow). Since CST sprouting rostral to the injury relates to improved locomotor function,[62,63] we studied the CST sprouting area (collaterals originating from the CST) immediately rostral to the first hemisection (segments T2 to T7) (Figure 5E).

The serotonergic (5HT) descending tracts can contribute to and improve voluntary motor activity after SCI.[12,64] Therefore, we studied the preservation of 5HT-positive fibers between hemisections (Figure 5F, left, white dotted lines indicate rostral and injury area) in the three experimental groups. However, we did not observe any significant differences in the density of 5HT fibers between groups (Figures 5F and 5G).

We then explored myelin preservation along the injured area by myelin binding protein (MBP) immunostaining, and we found an enhanced myelinated area in NaChBac mice compared to control mice (Figure 5H). Accordingly, we found better preservation of

NaChBac-GFP, $^{****}p < 0.0001$. (E) Graphs depicting the percentage of correct placement of both hindpaws of animals from all treatment groups in the ladder beam test 1 day before sacrifice (left), and the percentage of animals from each treatment group receiving the scores for the ladder beam test (right). Two-way ANOVA followed by Tukey's *post hoc* test, $^{**}p = 0.0095$. (F) Graphs depicting response-evoking threshold force (g) at which animals retracted their paws. One-way ANOVA followed by Tukey's *post hoc* test. Data presented as mean ± SEM.

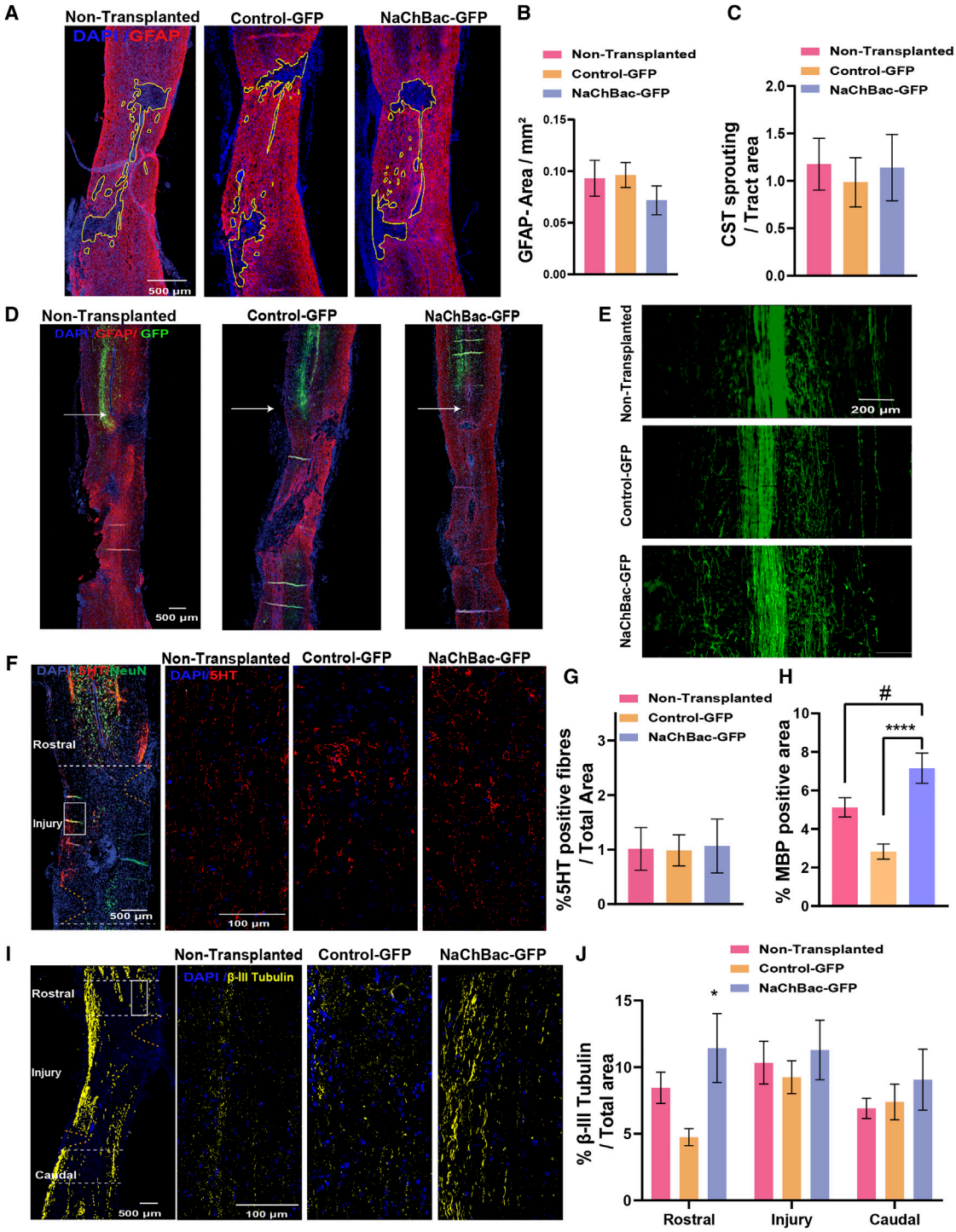

Figure 5. Evaluation of injured area and neuronal fiber preservation after transplantation of NaChBac-expressing DRGs

(A) Representative images of horizontal spinal cord sections for GFAP staining (red) and GFAP-negative injured area identification (delimited in yellow) in all treatment groups. GFAP, red; DAPI, blue. Scale bar, 500 µm. (B) Quantitation of the GFAP-negative injured area normalized to the total area from (A). One-way ANOVA followed by Tukey's *post hoc* test. (C) Quantification of CST sprouting normalized to tract area by GFP detection from (E). One-way ANOVA followed by Tukey's *post hoc* test. (D) Representative images of GFP (traced CST) rostral to the injury in all treatment groups. White arrows indicate complete degeneration of traced CST. GFP, green. Scale bar, 500 µm. (E) Representative images of the CST (center, parallel bundles) and sprouting (collaterals) in all treatment groups. GFP, green. Scale bar, 200 µm. (F) Representative images of

(legend continued on next page)

neuronal fibers in the spinal cord, detected using β-III-tubulin staining, rostral to the injury (Figures 5I and 5J).

Collectively, we find that NaChBac-GFP transplant improves the myelin and rostral neuronal fiber preservation without significantly improving CST sprouting nor 5HT fibers in the chronic stage of SCI.

NaChBac increases the excitatory profile of host neurons within the relay zone and immediately caudal to the injury

Finally, we studied whether the reported improvement in locomotor function of NaChBac-GFP-transplanted mice was associated with altered synaptic inputs of host neurons and their activity.

First, we analyzed the effect of DRG transplants on the neuroprotection of host neurons following SCI. No significant differences in endogenous neuronal survival rates between the experimental groups were found (as measured by NeuN quantification; Figures S2C and S2D), suggesting that Control-GFP or NaChBac-GFP DRG transplants failed to reduce the neuronal death after SCI.

We next explored whether the transplantation of NaChBac-GFP-expressing dissociated DRGs could influence neuronal activity within the relay zone (between hemisections). We studied the excitatory and inhibitory profiles of endogenous neurons within the hemisections and caudal to the injury by quantifying the number of excitatory vesicular glutamate transporter 1/2 (VGLUT1/2)- and inhibitory vesicular GABA transmitter (VGAT)-positive contacts in each neuron. VGLUT1 is a marker of pre-synaptic contacts from the CST and primary afferent fibers, while VGLUT2 is a pre-synaptic marker in supraspinal (other than CST) and propriospinal contacts.[65,66] VGAT is a transporter for the inhibitory neurotransmitter GABA (γ-aminobutyric acid).[67] Since the double-staggered hemisection model disrupts all supraspinal input after the second hemisection, we considered VGLUT1 expression caudal to the injury as almost exclusive to primary afferent fibers and VGLUT2 to propriospinal neurons.[68] At the injury site, we uncovered an increase in the number of VGLUT2 contacts (Figure 6A) per neuron in NaChBac mice compared to control groups (Figure 6B). However, no significant change in the number of VGAT contacts (Figure 6C) was detected (Figure 6D). This indicates that NaChBac-expressing DRG transplant could induce synaptic contacts between supraspinal (other than CST) and propiospinal neurons, propiospinal and propiospinal neurons, or both.

Caudal to the injury, we also observed increased VGLUT2 contacts per neuron in the NaChBac-expressing DRG-transplanted group compared to control groups (Figures 6E and 6F). Similar results were obtained when analyzing VGLUT1-positive contacts per neuron in the same region (Figures S4A and S4B). Strikingly, our analysis of VGAT signal immediately caudal to the injury revealed an expression profile almost opposite to VGLUT2, showing a significant decrease in the number of VGAT contacts per neuron in the NaChBac-expressing DRG-transplanted group compared to control (Figures 6G and 6H).

We also measured the VGLUT1/2 signal within the lumbar segments of the spinal cord. Given the specific distribution of VGLUT1/2 across the laminae,[65] we studied the VGLUT2-positive area in cross sections at the lumbar enlargement (L1–L6), differentiating between different spinal cord laminae I–X, as represented in Figure 6I (upper left), but we did not detect differences between groups (Figure 6J) nor in the VGLUT1-positive area (Figures S4C and S4D).

Our findings suggest an altered excitation/inhibition balance biased toward excitation within both the injury relay zone and the immediately caudal-to-injury region in the NaChBac-expressing DRG-transplanted mice. Along with increased neuronal fiber preservation, we propose that the transplant of NaChBac-expressing DRG neurons stimulates relay circuit activity, causing reorganization in the host excitatory/inhibitory input ratio, which is maintained immediately caudal to the injury and contributes to an improvement in the locomotor function after complete SCI.

DISCUSSION

When transplanted within the injured site, rat neonatal DRGs genetically modified to overexpress NaChBac rescued locomotor function in a severe SCI model. NaChBac dissociated DRGs could promote early establishment of detour circuits within descending tracts and propriospinal interneurons, which relay information as seen with a maintained excitatory input and neuronal activity immediately below the injury.

NaChBac expression decreases the neuronal activation threshold and produces long depolarization waves in CNS neurons.[36–41] The expression of NaChBac in DRG neurons increased their intrinsic activity and prompted a slow activating and inactivating inward current characteristic of this sodium channel at hyperpolarizing voltages around −50 mV. In both CNS[41] and DRG neurons, NaChBac increases intracellular Ca^{2+} influx and levels of intracellular cAMP in DRG neurons. Ca^{2+} and cAMP intracellular influx influences fundamental physiological processes such as cell survival, differentiation,[42] and initiation/propagation of nerve impulses.[69,70] Therefore, NaChBac expression may contribute to accelerated neuron maturation[41] or modulate neuronal plasticity.[71,72] In adult neuronal repair, the conditioning lesion paradigm (a phenomenon where a previous insult to the peripheral axon of DRG neurons leads to a switch in the regenerative capacity

preserved 5HT (red) fibers within the SCI in all treatment groups. DAPI, blue; NeuN, green. Scale bars, 500, 100 μm. (G) Quantification of 5HT preservation (serotonergic) fibers in the lesion site from (F). One-way ANOVA followed by Tukey's *post hoc* test. (H) Graphical representation of MBP staining preservation along the injury. One-way ANOVA followed by Tukey's *post hoc* test; $^{\#}p = 0.01$, $^{****}p < 0.0002$. (I) Representative images of β-III-tubulin-positive (yellow) preserved fibers rostral to the injury in all treatment groups. β-III-tubulin, yellow; DAPI, blue. Scale bars, 500, 100 μm. (J) Graphical representation of preserved β-III-tubulin-positive fibers (yellow in I) rostral to, within the injury site, and caudal to the injury site from (I). One-way ANOVA followed by Tukey's *post hoc* test, $^{*}p = 0.03$. Unless specified, $n = 4–7$. Data presented as mean ± SEM.

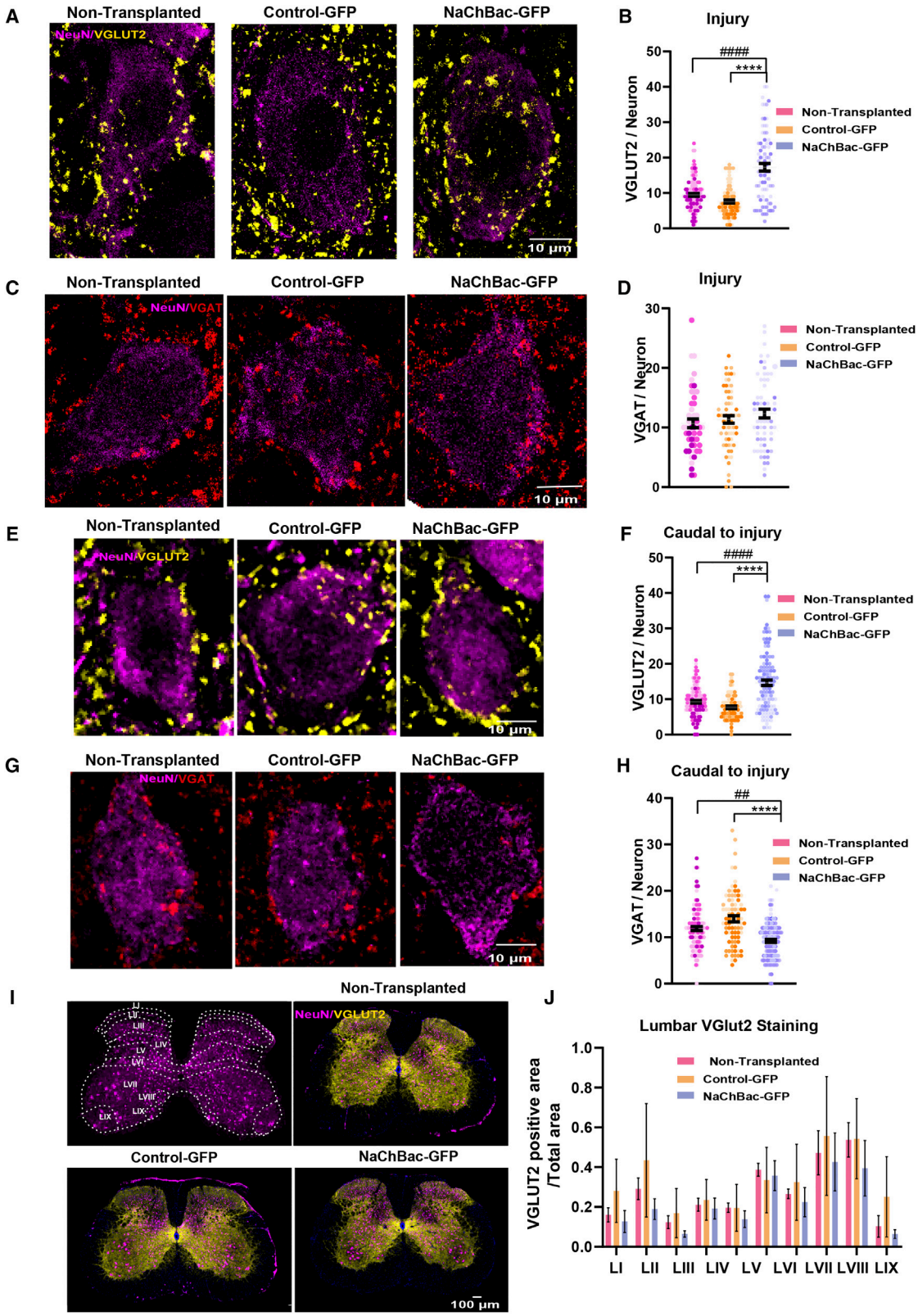

(legend on next page)

of the central axon) is mediated by the upregulated expression of several regeneration-associated genes after increased levels of intracellular Ca^{2+} and cAMP within DRG neurons.[73–76] Since NaChBac expression increased both Ca^{2+} and cAMP in DRGs, we hypothesized that NaChBac could induce a pro-regenerative state of DRG neurons transplanted within the SCI.

NaChBac prompts neuronal survival by increasing neuronal excitability.[37–39] In neuroblastoma cells, NaChBac expression increased proliferation and promoted cell survival. Bcl-2 regulates Ca^{2+} homeostasis,[77] while Ca^{2+} influx activates AKT signaling,[43] which, in turn, also modulates the mTOR complex.[78] We confirmed an increase in p-AKT and p-mTOR after NaChBac expression, suggesting the induction of Ca^{2+}-dependent signaling. The mTOR pathway is induced after PTEN downregulation,[79] associated with increased CST regeneration and functional recovery after SCI.[15,64] Indeed, mTOR activation represents a relevant pathway for neuronal survival and regeneration after SCI.[80] We postulate that AKT/mTOR axis activation by NaChBac expression can aid in overcoming inhibitory responses after transplantation of NaChBac-GFP dissociated DRGs. Indeed, NaChBac expression induced an increase in the secretion of neurotrophic factors in dissociated DRGs *in vitro*, including relevant neurotrophins such as BDNF, GDNF, and NGF. This suggests that NaChBac-transplanted cells can contribute to and promote an environment that supports neuronal preservation and synaptic plasticity, which could contribute to further neuronal functional recovery.[81] BDNF has been shown to enhance neuronal survival and increase plasticity of tracts, including the CST.[82] NGF is known to have a neuroprotective effect and, when overexpressed in transplanted neural stem cells, modulates injury environment and promotes functional recovery.[83] VEGF, which promotes revascularization after SCI, can also promote functional recovery by preventing secondary degeneration after SCI.[84] Similarly, GDNF improves neuronal survival and axonal regeneration and inhibits secondary damage post-SCI.[85] IGF-1 has been shown to exhibit neuroprotective effects by preventing apoptosis,[86] whereas GM-CSF can attenuate glial scar formation.[87] Subcutaneous administration of PDGF-AA has also been shown to contribute to functional recovery by increased oligodendrocyte survival and therefore increased myelination and motor neuron survival.[88]

DRG neurons transplanted within the injury site survived for at least 14 days and exhibited long axons; however, we did not observe transplanted cells after 2 months. A low number of DRG neurons surviving following xenotransplantation were previously reported by the Silver laboratory, where adult mouse DRG neurons transplanted in adult rats displayed a significant decrease in survival 2 weeks after transplantation.[31,32]

While increased endogenous neuronal activity induced by NaChBac expression improved cell survival during development[38] and integration into adult circuits,[39] these studies do not involve an injury. We found a higher number of NaChBac-expressing cells filling the injured tissue following NaChBac-GFP transplantation compared to Control-GFP transplantation 14 days after the injury. Several studies suggest that neuronal activity plays a crucial role in neuron migration during development[89,90]; therefore, NaChBac could provide additional migratory capacity to neurons but not glial cells. Indeed, upon NaChBac-GFP transplantation, NaChBac DRG neurons migrated away from the injury epicenter in the rostral direction. These enhanced migratory properties could provide additional benefits by maintaining activity near the degenerating tracts rostral to the injury. Activity-based stimulation can also improve CST remodeling after SCI.[56,57] Our findings report promising results, with increased preservation of the injured CST and the formation of a more permissive environment in mice transplanted with NaChBac-expressing DRG neurons (Figures S2A and S2B). This may occur due to the migration of neurons near the CST and a permissive environment formed by the glial cells transplanted alongside DRG neurons from the dissociated DRG cultures.

The double-staggered lateral hemisection injury model offers a robust scenario to study spontaneous recovery because spared axons between the two injured segments can form short detour circuits with propriospinal interneurons that relay information, while all descending tracts become severed.[5,13,58,91] A steady increase in locomotor performance was observed based on the ladder beam assay and BMS scores of mice transplanted with NaChBac-expressing dissociated DRGs 2 months after injury. Although NaChBac-expressing dissociated DRGs enhanced CST sprouting and preservation 2 weeks after injury, no differences between mice were observed 2 months later.

Figure 6. Excitatory and inhibitory synaptic terminals within injury and immediately caudal to injury after transplantation of NaChBac-expressing DRG neurons

(A) Representative images illustrating NeuN (magenta) and VGLUT2 (yellow) contact sites with neurons within the injury site in all treatment groups. Scale bar, 10 μm. (B) Quantification of VGLUT2 contacts per neuron, from (A). One-way ANOVA, Kruskal-Wallis test. Non-transplanted vs. NaChBac-GFP, $^{\#\#\#\#}p < 0.0001$; Control-GFP vs. NaChBac-GFP, $^{****}p < 0.0001$. (C) Representative images illustrating NeuN (magenta) and VGAT (red) contact sites with neurons within the injury in all treatment groups. Scale bar, 10 μm. (D) Quantification of VGAT contacts per neuron, from (C). One-way ANOVA, Kruskal-Wallis test. (E) Representative images illustrating NeuN (magenta) and the VGLUT2 (yellow) contacts with neurons immediately caudal to the SCI in all treatment groups. Scale bar, 10 μm. (F) Quantification of VGLUT2 contacts per neuron immediately caudal to injury, from (E). One-way ANOVA, Kruskal-Wallis test. Non-transplanted vs. NaChBac-GFP, $^{\#\#\#\#}p < 0.0001$; Control-GFP vs. NaChBac-GFP, $^{****}p < 0.0001$. (G) Representative images illustrating NeuN (magenta) and the VGAT (red) contacts with neurons immediately caudal to the SCI in all treatment groups. Scale bar, 10 μm. (H) Quantification of VGAT contacts per neuron, from (G). One-way ANOVA, Kruskal-Wallis test. Non-transplanted vs. NaChBac-GFP, $^{\#\#}p = 0.0038$; Control-GFP vs. NaChBac-GFP, $^{****}p < 0.0001$. Each dot represents an individual neuron in (B), (D), (F), and (H). Unless specified otherwise, $n = 4$. (I) Representative images showing the identified layers of VGLUT2 staining in the lumbar spinal cord in all treatment groups; NeuN, magenta; VGLUT2, yellow; and DAPI, blue. Scale bar, 100 μm. (J) VGLUT2-positive area relative to total area quantified in the lumbar region of the spinal cord (L1–L6) ($n = 4$). Two-way ANOVA followed by Tukey's *post hoc* test. Data presented as mean ± SEM.

This indicates that early remodeling with alternative neuronal connections above CST innervation contributed to later functional recovery. Since we failed to detect differences between treatment groups upon 5HT fiber staining, we discarded the raphespinal contribution. Nevertheless, given the significant overall increase in the preservation of myelin across the injury and of β-III-tubulin fibers rostral to the injury, we hypothesized that the reticulospinal, rubrospinal, and/or vestibulospinal tract could contribute to the descending input. The improved locomotion observed in mice transplanted with NaChBac-GFP dissociated DRGs could relate to improved overall myelin and neuronal fiber preservation rostral to the injury and increase in VGLUT2 contacts per neuron. We hypothesized that, without major descending tracts after SCI, neuronal fibers would form relay connections with propriospinal interneurons.

During development, pruning of connections is associated with loss of neuronal activity.[92] Interestingly, SCI leads to a loss of supraspinal inputs[4] and remodeling of neurotransmitter phenotype from excitatory to inhibitory,[17] accompanied by neuronal inactivation leading to locomotor deficits.[16] However, SCI can induce circuit rearrangements by sprouting and/or forming relay circuits to transmit information below the injury to maintain neuronal function.[9,11–13] Increased neuronal activity contributes to neuroplasticity,[93] neuronal rewiring,[94] and functional recovery after SCI.[14] These findings highlight the importance of maintaining neuronal activity caudal to the injury to support the function beneath the injury and improve the formation of detour circuits after SCI.[95] Supraspinal neurons that project into the spinal cord (except CST) and propriospinal neurons express VGLUT2.[65,66] Since descending inputs are interrupted, the double hemisection model enables the formation of relay circuits within the injury site and ensures the exclusivity of VGLUT2 expression to propriospinal neurons caudal to the injury.[68] In contrast, the inhibitory profile can be studied through VGAT expression.[67] We found no changes in endogenous neuronal preservation between all treatment groups; rather, the number of VGLUT2 excitatory contacts received by each neuron significantly increased following the transplantation of NaChBac-expressing dissociated DRGs within the relay zone and immediately caudal to the injury compared to both control groups. We encountered a similar increase in VGLUT1 excitatory inputs immediately caudal to the injury in mice transplanted with NaChBac-expressing DRG neurons compared to both control groups, arising from preserved primary afferents. Within the relay zone, it remains unclear whether the increase in VGLUT2 contacts derives from an increase in supraspinal input, an increase in the relay activity of propriospinal neurons, or both. Our study revealed the maintenance of this increase in VGLUT2 contacts immediately caudal to injury, attributed to propriospinal neurons by virtue of this model.

Notably, we did not observe changes in VGAT expression within the relay zone; rather, we discovered a significant decrease in VGAT expression in NaChBac-GFP mice immediately caudal to the injury compared to both control groups. Together, this suggests that NaChBac-GFP increased the activity in the relay zone due to preserved VGLUT2-positive descending tracts, relay circuit formation with the propriospinal interneurons, or both, and given the maintenance of this profile immediately caudal to the injury, our data suggest a role for short propriospinal neurons in the relay input immediately caudal to the injury. These data suggest that mice transplanted with NaChBac-expressing dissociated DRGs maintain relay activity below the injury. The decrease in VGAT expression and increase in VGLUT2 expression can ultimately explain functional improvements.

Severe SCI induces rewiring in denervated spinal cord segments, which can lead to undirected and abnormal plasticity in the lumbar region of the spinal cord.[68] Since we did not observe differences in VGLUT2 nor VGLUT1 staining in the lumbar region between treatment groups, we hypothesized that mice transplanted with NaChBac-expressing DRG neurons only maintain a detour circuit activity immediately caudal to the injury, thereby preventing undirected plasticity in the lumbar region and promoting functional recovery. Enhancing neuronal activity mimicking NaChBac-mediated excitation, achieved, for instance, by using sodium channel activators such as veratridine and aconitine, which act by shifting and lowering the potentials at which the channels open and give rise to longer currents, would be employed as an alternative therapeutic strategy.[96] However, targeted delivery and adequate dosage with a controlled kinetics must be considered to prevent potential undesired effects.[97]

In conclusion, we describe the effect of transplanting dissociated DRGs with increased intrinsic activity provided by the expression of NaChBac after SCI. Our findings indicate that NaChBac-expressing dissociated DRGs maintain activity from supraspinal inputs and form detour circuits. Transplantation in a single-hemisection model leads to early CST preservation, and in a double-hemisection model shows a significant preservation of VGLUT2-positive descending inputs due to an increased relay circuit formation with propriospinal interneurons, maintained immediately below the injury. This reinforces the importance of maintaining the excitation/inhibition ratio immediately caudal to SCI, highlighting its role in enhancing the formation of relay circuits, and conveys the importance of developing new therapeutic strategies focused on that point.

MATERIALS AND METHODS

Culture of dissociated DRGs

DRGs were isolated from neonate rats at P3–P4, as previously described.[98] Briefly, DRGs were dissected from all medullar segments, pooled, and collected in cold Hank's balanced salt solution (HBSS). Residual spinal roots and nerves attached to the DRGs were removed. DRGs were digested with collagenase IA (no. C9891, Sigma) for 35 min, followed by 7 min digestion with Tryple (GIBCO cat. no. 12563-011). Digested DRGs were suspended in complete medium (MM: DMEM F12 + 10% fetal bovine serum [FBS] + 1% penicillin/streptomycin [P/S] and 2.5 ng/μL NGF [13257-019, Gibco]), mechanically dissociated with a 1,000 μL blue pipette tip, and plated on coverslips or plastic plates coated with poly-L-lysine (no. P2636, Sigma) 20 μg/mL overnight at 37°C and laminin (no. L2020, Sigma)

10 μg/mL for 3 h at 37°C at various densities, as described later. AraC (no. C1768, Sigma) (5 μM) was added after 16 h to reduce glial cell growth. Half the medium volume was refreshed every 3 days.

Stable NaChBac expression

Sequence coding for NaChBac fused to eGFP was obtained from the NaChBac FRSW plasmid (kindly provided by Dr. Carlos Lois)[39] and cloned into the pLL3.7 lentiviral vector (Addgene, no. 11795). For lentiviral production, the HEK293T cell line was transfected with the pLL3.7-NaChBac-eGFP construct or pLL3.7 empty vector together with amphitropic packing and envelope-containing constructs using the calcium phosphate method,[99] as described in Sánchez-Huertas et al. and Rubinson et al.[100,101]

Dissociated DRG neurons or the stable mouse neuroblastoma N2A cell line were transformed to overexpress NaChBac-eGFP (NaChBac-GFP) or empty vector containing eGFP (Control-GFP) by infecting the cell cultures 4 h after plating with pLL3.7-NaChBac-eGFP or pLL3.7 empty vector lentiviral particles at MOI 10. For calcium imaging experiments, dissociated DRG cultures were transformed to overexpress pLL3.7-NaChBac-mScarlet (NaChBac-mScarlet) or pLL3.7-mScarlet (Control-mScarlet) to distinguish from Fluo-4AM.

N2A cell survival

N2A cells expressing NaChBac-GFP or Control-GFP were plated at a density of 300,000 cells/well in a six-well plate to create a proliferation curve. Cells were trypsinized and counted in a Neubauer chamber on days 2, 3, 4, and 5. Trypan blue (15250061, Thermo Fisher Scientific) was added to highlight dead cells. For hypoxic stimulation, cells were placed in a hypoxia chamber set at 1% oxygen for 24 h, trypsinized, and counted by adding Trypan blue.

Western blotting

Total protein from N2A cells was extracted using lysis buffer containing 1× Protease Inhibitor Cocktail (11836153001, Roche Diagnostics), 50 mM Tris-HCl (pH 7.5), 150 mM NaCl, 1% NP-40, and 1 mM orthovanadate. Protein concentrations were determined using the BCA Protein Assay Kit (no. 23225, Thermo Fisher Scientific). Equal amounts of protein were separated by 10% SDS-PAGE, transferred to a polyvinylidene fluoride (PVDF) membrane, and blocked with 5% bovine serum albumin in T-BST buffer (20 mM Tris-HCl [pH 7.4], 150 mM NaCl with 0.1% Tween 20) for 1 h at room temperature and incubated at 4°C overnight with the following primary antibodies: rabbit phospho-mTOR 1:1,000 (no. 2971, Cell Signaling), rabbit mTOR 1:1,000 (no. 2972, Cell Signaling), mouse Bcl2 1:100 (no. sc-7382, Santa Cruz Biotechnology), mouse phospho-AKT 1:1,000 (no. sc-293125, Santa Cruz Biotechnology), rabbit caspase 3 1:1,000 (no. 9622s, Cell Signaling), rabbit AKT 1:1,000 (no. 4691s, Cell Signaling), and mouse β-actin 1:10,000 (no. A1978, Sigma).

Signal detection was performed with a chemiluminescence kit (ECL Plus western blotting detection reagent; GE Healthcare) and bands were developed using the Uvi-Tech Alliance Q9 chemiluminescence imaging system. Relative protein expression was quantified using Uvi-Tec NineAlliance Q9 h software.

Electrophysiology recordings

Small-diameter (<30 μm) DRG neurons were recorded in voltage and current-clamp modes using an EPC10 amplifier controlled by Patchmaster software (HEKA Elektronik). Experiments were performed in whole-cell configuration at ≈22°C. Briefly, patch pipettes made from borosilicate glass with OD 1.5 mm × ID 1.17 mm (Warner Instruments) were pulled using a Flaming/Brown micropipette puller P-97 (Sutter Instruments) to have 2–5 MΩ resistance. Seal resistance was between 200 MΩ and 2 GΩ, and series resistance was compensated for around 80%.

GFP-positive DRG neurons at 72–96 h post-infection were selected using a fluorescence microscope (Axiovert 200 Inverted Microscope, Carl Zeiss). Extracellular solution contained 140 mM NaCl, 4 mM KCl, 2 mM $CaCl_2$, 2 mM $MgCl_2$, 10 mM HEPES, 5 mM glucose, 20 mM mannitol (pH 7.4 adjusted with NaOH). The pipette internal solution contained 144 mM KCl, 2 mM $MgCl_2$, 10 mM HEPES, and 5 mM EGTA (pH 7.2 adjusted with KOH).

Resting membrane potential was determined without current injection after establishing whole-cell access. One second current depolarizing pulses from 0 to 300 pA in 10 pA intervals were applied to calculate the rheobase and firing frequency. The minimum current required to evoke the first action potential was considered the current rheobase. The action potential parameters were measured in the action potential fired at the minimum current injected using 10 ms depolarizing pulses from 0 to 300 pA in 10 pA steps. The action potential's voltage threshold (Vth) was set when the upstroke slope was ≥10 V/s. The action potential amplitude was calculated between the resting membrane potential and the action potential peak.

A series of 300 ms voltage steps from −80 to 60 mV in 10 mV intervals was applied for voltage-clamp recordings (Vh = −60 mV). Data were acquired at 20 kHz for all the protocols. Only one cell per dish was recorded.

Calcium live imaging

Four days after seeding at a density of 21,000 cells/cm^2 in 24-well plates with a glass surface (662000-06, Greiner Bio-One) and infecting with either NaChBac-mScarlet or Control-mScarlet, the cultures were treated with Fluo-4AM (no. F14201, Thermo Fisher) at 3 μM for 30 min according to the manufacturer's instructions. A Leica TSP-SP8 confocal microscope was used, as it includes resonant scanning mirrors for real-time live imaging.[102] Recording started around 10–20 s before depolarization by directly adding 100 mM KCl into the well and continued for 60 s.

The change in fluorescence of the cells was determined using LasX software. Data were screened so that neurons not responding to depolarization by KCl were discarded from the analysis.

cAMP level determination

Four days after infection with NaChBac-GFP or Control-GFP, cAMP was extracted from cells using the perchloric method.[103] The chromatographic conditions for cAMP detection were optimized to the XBridge C18 2.1 × 75, 2.5 μm (no. 186005626, BEH Technology, Waters, USA), based on the work of Wojnicz et al.[104] The mobile-phase composition was component A, 0.1% formic acid in water; component B, 100% acetonitrile. The conditions for the chromatographic run were flow rate 0.4 mL/min; gradient 0.5 min 100% A, 1 min 10% A, 2.2 min 10% A, 2.3 min 100% A, 3.5 min 100% A. Volume injected was 25 μL.

Secretome analysis

For secretome analysis, *in vitro* dissociated DRG cultures were used. Three days after infection with NaChBac-GFP or Control-GFP, culture medium was changed to low-serum medium: MEM + 2% FBS + 1% P/S. Medium was collected 24 h later and stored at −20°C until use. Array analysis was performed using Rat Growth Factor Array 1 (no. AAR-GF-1-2, RayBiotech, GA, USA). Briefly, undiluted culture medium was directly incubated over a membrane well, followed by washes and antibody incubations, and visualized using the Uvi-Tech Alliance Q9 chemiluminescence imaging system. Data were analyzed as per the manufacturer's instructions (n = 2). BDNF secretion was used to additionally validate these data by using an ELISA kit (CC-SEA011Hu, Biogen Científica, Madrid, Spain) for BDNF in a different set of samples (n = 2). Similar data were obtained when medium from N2A culture was employed using the same array and the BDNF ELISA (data not shown).

SCI and DRG transplantation

All *in vivo* procedures were performed in female C57BL/6 mice (approx. 20 g, 8 weeks of age) bred at the Animal Experimentation Unit of the Príncipe Felipe Research Institute (CIPF, Valencia, Spain). The maintenance and use of all animals followed guidelines established by the European Communities Council Directive (86/609/ECC) and Spanish Royal Decree 53/2013. All experimental procedures were approved by the Animal Care and Use Committee of the Research Institute Prince Felipe (2020/VSC/PEA/0120). The experimental protocol included humane endpoint criteria when severe signs of distress were observed. Mice were housed under standard temperature conditions with controlled 12 h light/dark cycles with *ad libitum* access to food and water. Animals were managed by professionally trained staff. Female mice were used for this study due to shorter urinary tract and decreased infection susceptibility.[105]

Two models of SCI by hemisection were performed. To induce SCI, mice were subcutaneously administered 5 mg/kg morphine 30 min before the surgery, and anesthesia was maintained throughout the surgery by a continuous flow of 2% isoflurane and oxygen of 1 L/min.

Single T8 hemisection was performed as described in Kathe et al.[106] Briefly, a laminectomy was performed to expose T8, and a lateral right hemisection was performed using a micro scalpel blade (no. 72-2201, Sharpoint Angiotech). The incision was performed twice to ensure complete severing. The muscle and skin layers were then separately sutured using 4/0 monosyn sutures (no. G2022004, Braun). Animals for the single-hemisection approach were distributed into two groups: (1) SCI and Control-GPF-expressing dissociated DRG transplant (Control-GFP) and (2) SCI and NaChBac-eGFP-expressing dissociated DRG transplant (NaChBac-GFP); n = 8–9 animals/group for histological analysis.

Complete injury was performed by the T7–T10 double unilateral complete hemisection model as described by Chen et al.[5] After T7–T10 laminectomy, an incision was made using a micro scalpel blade (no. 72–2201, Sharpoint Angiotech) on the right T7 side and the left side at T10 level until midline. These incisions were performed twice to ensure complete severing. Animals for the double-hemisection approach were placed into three groups: (1) SCI and no cell transplant (non-transplanted), (2) SCI and Control-GPF dissociated DRG transplant (Control-GFP), and (3) SCI and NaChBac-eGFP dissociated DRG transplant (NaChBac-GFP); n = 8–12 animals/group for locomotion analysis; n = 4–7 for histological analysis.

Transplants were performed immediately after the incision in a single injection at T8 (150,000 cells in 3 μL volume) using a Hamilton syringe (no. 80308) coupled to a siliconized sharpened glass capillary attached to a Nanoliter injector (Harvard Apparatus). Cells were infused at 2 μL/min and allowed to deposit for 2 min before the capillary was removed.

All animals were subcutaneously administered buprenorphine twice daily (0.1 mg/kg) for 4 days after surgery and enrofloxacin once a day for a week after surgery (5 mg/kg). Bladder drainage was performed twice daily until recovery or the experimental endpoint. The immunosuppressant cyclosporine (once a day, 20 mg/kg) was administered 1 day before transplantation until endpoint.

Neuroanatomical tracing

Tracing of the hindlimb CST was performed as described by Hilton et al.[50] at coordinates AP −0.50, ML ±1.50, and DV −0.70 from bregma. In the model of complete SCI by double hemisection, 1.5 μL of pAAV-hSyn-EGFP (no. 50465, Addgene) (titer 3.75×10^{11}) was injected into the right hemisphere and 1.5 μL of pAAV-hSyn-RFP (no. 22907, Addgene) (titer 3.75×10^{11}) into the left hemisphere. In the model of SCI by single hemisection, 1.5 μL of pAAV-hSyn-RFP was injected into both the right and the left motor cortex.

Locomotion analysis

Functional outcomes were evaluated by locomotor recovery using BMS[59] twice a week. The horizontal ladder beam test[60] was also performed to assess hindlimb coordination. Animals were recorded crossing a horizontal ladder for at least three rounds.[107] After carefully considering the videos, we employed a scaling method adapted from Cummings et al.,[60] where score values were assigned to the terms described instead of names.

Von Frey test

The Von Frey allodynia test was performed as described, following the "ascending stimulus" method described in Deuis et al.[108] Briefly, Von Frey filaments in ascending order were applied an equal number of times (three) for each paw until a withdrawal was recorded and assigned as the "mechanical withdrawal threshold" (g). The mean of each paw was then plotted.

Tissue processing, tissue imaging, and analysis

At experimental endpoints, animals were anesthetized with fentanyl (0.05 mg/kg) and pentobarbital (100 mg/kg) via intraperitoneal injection. Tissue fixation was achieved by transcardial perfusion with 0.09% w/v saline, followed by 4% paraformaldehyde in 0.1 M phosphate buffer. Spinal cords were dissected, kept in 4% paraformaldehyde solution for 4 h, and stored in 0.1 M phosphate buffer containing 0.02% sodium azide.

Thoracic segments T2–T12 were obtained and either cryopreserved in 30% sucrose for inclusion in Tissue-Tek OCT (Sakura Finetek Europe BV) and stored at −80°C until sectioning or included in paraffin. Paraffin-embedded tissue was sectioned in longitudinal sections (8 μm) and collected on gelatin-coated slides in five series. Cryopreserved tissue in longitudinal or coronal (as specified) 35 μm sections were collected in six series in wells containing cryoprotectant solution (25% v/v glycerol, 30% v/v ethylene glycol in 0.1 M phosphate buffer).

Immunohistochemistry

Sections embedded in paraffin were first heated at 65°C for 30 min to remove excess paraffin, followed by rehydration and deparaffinization carried out in the Leica Autostainer. Next, an antigen retrieval procedure was performed: sections were incubated for 25 min in Tris-EDTA buffer (10 mM Tris base, 1 mM EDTA solution, 0.05% Tween 20 [pH 9]) at 97°C.

In the case of cryopreserved tissue, no previous steps were performed.

Sections were then blocked and permeabilized with a solution of 10% FBS, 5% horse serum, and 0.1% Triton X-100 in PBS for 1 h at room temperature and incubated with primary antibody solution overnight in a humid chamber. Primary antibodies were employed using the following dilutions: rabbit anti-GFAP (1:600, Z0334, DAKO), mouse anti-β-III-tubulin (1:400, 11-264-c100, EXBIO), chicken anti-GFP (1:1,000, ab13970, Abcam), guinea pig anti-RFP (1:1,000, 390004, Synaptic Systems), rabbit anti-serotonin (1:400, S5545, Sigma), guinea pig anti-VGLUT1 (1:400, 135305, Synaptic Systems), rabbit anti-VGLUT2 (1:400, 135402, Synaptic Systems), rabbit anti-VGAT (1:400, 131002, Synaptic Systems) and chicken anti-NeuN (1:600, ABN91, Merck Millipore), rabbit anti-Iba-1 (1:400, 019-19741, FUJIFILM Wako Chemicals Europe), rabbit anti-MBP (1:400, ab69863, Abcam), and mouse anti-fibronectin (1:400, sc-8422, San Cruz).

Conjugated secondary antibodies Alexa Fluor 488, 555, and 647 were used against the respective IgG for 1 h at room temperature. Slides were counterstained with DAPI (1:1,000, no. D9542, Sigma) and mounted with Mowiol (no. 81381, Sigma).

Images from the histological analysis were acquired from either an Aperio Versa scanner or Zeiss Apotome, visualized, and analyzed using a Leica AperioScope and ImageJ.

Quantification of cell number

The total number of cells/neurons (Figure S1C) was counted manually across an entire series of each animal and then multiplied by the total volume of the series to estimate the total number of cells in the entire spinal cord. In some animals, the total number of cells was counted in clarified spinal cords (clarified following the protocol described by Tainaka et al.[109]), imaged using a Zeiss Light Sheet fluorescence microscope, and visualized using IMARIS software. Each analysis was first normalized to the mean of its control to compare the analysis.

Rostral migration

Images of (cryopreserved) longitudinal sections were taken using the Aperio Versa scanner and visualized using AperioScope software. The lesion and injection center were manually marked as the site as per the damage to the tissue, and a horizontal line to the farthest transplanted cell (GFP positive) in both directions, caudal and rostral, was drawn.

CST passing through the transplant

The transplanted area was traced manually in ImageJ (Figure S2A), and the area of CST passing through this area was calculated by applying the same threshold for all sections. Data were normalized to total transplanted area.

CST preservation after lesion

To calculate the positive pixels in the CST after injury, the midpoint of every injury (identified by the degradation of the CST and the tissue) was marked as 0 (no pixel value). Next, the same area and threshold values were applied to the images. Using Dynamic ROI Profiler in ImageJ, the positive pixels for CST per column of the image were obtained using the following equation X*H/255 = Y, with X being the data provided by the histogram, H the height of the selected area in pixels, 255 the maximum positive pixel value, and Y the positive pixels. These data were then represented as positive pixels/micrometer of the image from the midpoint of the injury.

CST sprouting analysis

CST sprouting analysis in the T7–T10 double lateral hemisection model was analyzed in the following manner: positive area of the descending CST fibers (GFP expressing) transduced by the injection of the AAV9-Synaptophysin-GFP particles in the right hemisphere of the motor cortex area was measured and normalized to the traced tract area. The analysis was carried out in an entire series of animals throughout the dorsoventral axis from T3 to T6 (rostral to the lesion) in at least seven paraffin longitudinal slices per animal.

Coronal (cryopreserved) sections immediately rostral to the lesion site (T3) were analyzed for the single lateral hemisection model.

The positive area of CST fibers (RFP expressing) was normalized to the CST traced area.

GFAP-negative area

The injured and scarred area was characterized by the delimiting border-forming astrocytes.[110,111] The extension of the scar was taken as a GFAP-negative area delimited by the GFAP-positive border and manually traced using the AperioScope software. Analysis was performed in paraffin longitudinal sections of the T2–T13 zone in at least six or seven slices throughout the dorsoventral axis of the spinal cord per animal. Values were normalized to the total tissue area.

GFAP expression analysis

Since GFAP expression is upregulated in reactive astrocytes, to determine the reactivity in astrocytes, we used GFAP immunoreactivity and measured the mean intensity of the area expressing GFAP surrounding the injury. Briefly, a border delimiting the injury area was manually traced (thickness of 100 μm from injury) and the mean intensity of that area was measured in ImageJ. This intensity was then normalized to GFAP immune-reactivity intensity away from the injury site. Analysis was performed in paraffin longitudinal sections of the T2–T13 zone in at least six or seven slices throughout the dorsoventral axis of the spinal cord per animal.

Inflammatory microglia profile analysis

Iba-1 staining was used to study the inflammatory profile of microglia based on their morphology.[112] ImageJ was used to obtain the circularity of each Iba-1^+ cell. According to their circularity, Iba-1^+ cells were then divided into two subtypes: (1) circular Iba-1^+, $c < 0.25$, or (2) ramified Iba-1^+, where $c > 0.25$. At least six images per section and three sections per animal were obtained around the injury area for this analysis.

Neuronal fiber analysis

The global preservation of neuronal fibers was identified by β-III-tubulin immunostaining rostral and caudal to the injury and within the injury, while excluding somas in the gray matter. Preservation of serotonin fibers was evaluated by 5HT immunostaining. Paraffin longitudinal sections were stained and evaluated in an entire series for every animal. A positive signal was measured by applying the same threshold for images taken at the same intensity and exposure at 1 mm segments for β-III-tubulin or 1.5 mm for 5HT staining in the rostral region (including T6) and caudal region (including T11) as well as in the lesion site (T7–T10). Each of these measurements (in pixels/mm^2) was expressed as a percentage of positive area normalized to the total area analyzed.

Myelin preservation analysis

The global preservation of myelin was analyzed using MBP immunostaining, measuring the positive signal, applying the same threshold for all images, taken at the same intensity and exposure, in a region of interest starting from 1 mm rostral to the injury epicenter to 1 mm caudal (including segments T6–T11), measured in pixels/mm^2 and expressed as a percentage of positive area normalized to the total area analyzed. At least five paraffin longitudinal sections were stained and evaluated in every animal.

Fibronectin expression analysis

Fibronectin staining was employed as a method to analyze fibrotic scarring within the injury site (segments T7–T10). The presence of fibronectin was analyzed by measuring fibronectin-positive signal by applying the same threshold for images taken at the same intensity and exposure. Each of these measurements (in pixels/mm^2) was expressed as a percentage of positive area normalized to the total area analyzed. At least five paraffin longitudinal sections were stained and evaluated in every animal.

NeuN quantification

NeuN staining was employed in and around the lesion site to quantify the number of neurons in longitudinal (paraffin) sections 1.5 mm rostral and caudal to the lesion and the lesion site. NeuNs were manually counted in delimited segments of 1.5 mm spinal cord length. We termed 1.5 mm immediately rostral to the lesion as Rostral 1 and 1.5 mm farther away as Rostral 2 and the same for Caudal 2 and 1 (Figure S2C). Data were expressed as the number of neurons quantified in each of these segments.[113]

Excitability and inhibitory neuronal input analysis

Longitudinal sections of the ventral zone were chosen to analyze contacts per neuron. Images were taken on a Leica TCS SP2 confocal microscope at a step size of 1 μm. VGLUT1/2 and VGAT immunostaining were used for excitatory and inhibitory input analysis when co-localized with NeuN-positive neurons. At least 15–20 neurons per section per zone (injury or immediately caudal) were analyzed in at least two sections per animal, in four animals per group. The values for every neuron were plotted individually as contacts per neuron.

For lumbar analysis, an entire series of coronal sections was analyzed. Spinal cords were divided into laminae I–X, as described by Alvarez et al.[65] The same threshold was applied in all sections for VGLUT1/2-positive areas for every lamina and then normalized to the total area of each lamina.

Statistical analysis

All statistical analysis was performed using GraphPad Prism software. The Shapiro-Wilk normality test was performed to ensure the dataset normality (Gaussian). Outliers were identified using ROUT's test ($Q = 1\%$). Comparisons between the two groups were carried out using the two-tailed t test. The Mann-Whitney test was performed for datasets that did not follow a normal distribution. One-way ANOVA was performed to compare more than two groups with single variables, followed by Tukey's post-test for typical datasets. Kruskal-Wallis one-way ANOVA with Dunn's *post hoc* correction was used for datasets that did not follow a normal distribution.

Two-way ANOVA was performed for repeated measurements with two variables, followed by Tukey's *post hoc* test. The confidence level for all tests was set as 95%. All bar plots are presented as the

mean ± SEM. The p values are represented as $^{*}p < 0.05$, $^{**}p < 0.01$, $^{***}p < 0.001$, and $^{****}p < 0.0001$. # and + were used following the same rule as * for different group comparisons.

Data availability

The raw data required to reproduce these findings will be available from the corresponding author upon request.

SUPPLEMENTAL INFORMATION

Supplemental information can be found online at https://doi.org/10.1016/j.ymthe.2024.03.038.

ACKNOWLEDGMENTS

The publication of the present research is part of the projects PID2021-1243590B-I100 and PID2021-126423OB-C21 (to A.V.F.M.), funded by MICIN/AEI/10.13039/501100011033/FEDER, Ministerio de Ciencia e Innovación – Agencia Estatal de Investigación co-funded with FEDER funds from the EU "Una manera de hacer Europa" and a RISEUP EU grant (ref. 964562) from the FetOpen H2020 program. The Generalitat Valenciana with the GVA PROMETEO/2021/031 (to A.V.F.M.) funded part of the equipment employed in this work and co-financed with ERDF funds (OP ERDF of Comunitat Valenciana 2014–2020) and the EU; Fondo Europeo de Desarrollo Regional (FEDER) included in the Programa Operativo FEDER de la Comunidad Valenciana 2014–2020. The Grisolia program from the GVA supported S.H. during her doctoral thesis. E.M.V.R. is a recipient of a UMH doctoral fellowship, funded by project PAR-UMH 2019 (to A.V.F.M.). The authors thank Dr. Frank Bradke for supporting S.H. to perform part of the microscopy images and analysis; Mara Mellado López for her technical support; the Microscopy Support Unit at the CIPF, Valencia (Spain); and Stuart P. Atkinson for English editing and critical review of the manuscript.

AUTHOR CONTRIBUTIONS

V.M.M., C.S.H., and S.H. presented and conceived the idea and designed experiments. S.H., G.P.S., E.M.V.R., E.L.M., A.A.A., and S.D. carried out experiments and data analysis. S.H., G.P.S., C.S.H., A.V.F.M., and B.M.R. contributed to critical discussions. S.H., V.M.M., and G.P.S. wrote the original draft of the manuscript. S.H., V.M.M., G.P.S., B.M.R., E.L.M., A.V.F.M., S.D., C.S.H., and E.M.V.R. edited the final manuscript version.

DECLARATION OF INTERESTS

The authors declare no conflict of interest.

REFERENCES

1. Ahuja, C.S., Wilson, J.R., Nori, S., Kotter, M.R.N., Druschel, C., Curt, A., and Fehlings, M.G. (2017). Traumatic spinal cord injury. Nat. Rev. Dis. Primers *3*, 17018. https://doi.org/10.1038/nrdp.2017.18.

2. Anjum, A., Yazid, M.D., Fauzi Daud, M., Idris, J., Ng, A.M.H., Selvi Naicker, A., Ismail, O.H.R., Athi Kumar, R.K., and Lokanathan, Y. (2020). Spinal Cord Injury: Pathophysiology, Multimolecular Interactions, and Underlying Recovery Mechanisms. Int. J. Mol. Sci. *21*, 7533. https://doi.org/10.3390/ijms21207533.

3. Aguayo, A.J., Rasminsky, M., Bray, G.M., Carbonetto, S., McKerracher, L., Villegas-Pérez, M.P., Vidal-Sanz, M., and Carter, D.A. (1991). Degenerative and regenerative responses of injured neurons in the central nervous system of adult mammals. Philos. Trans. R. Soc. Lond. B Biol. Sci. *331*, 337–343. https://doi.org/10.1098/rstb.1991.0025.

4. Dietz, V., and Müller, R. (2004). Degradation of neuronal function following a spinal cord injury: mechanisms and countermeasures. Brain. *127* (Pt 10), 2221–2231. https://doi.org/10.1093/brain/awh255.

5. Chen, B., Li, Y., Yu, B., Zhang, Z., Brommer, B., Williams, P.R., Liu, Y., Hegarty, S.V., Zhou, S., Zhu, J., et al. (2018). Reactivation of Dormant Relay Pathways in Injured Spinal Cord by KCC2 Manipulations. Cell *174*, 1599. https://doi.org/10.1016/j.cell.2018.08.050.

6. Fawcett, J.W., Curt, A., Steeves, J.D., Coleman, W.P., Tuszynski, M.H., Lammertse, D., Bartlett, P.F., Blight, A.R., Dietz, V., Ditunno, J., et al. (2007). Guidelines for the conduct of clinical trials for spinal cord injury as developed by the ICCP panel: spontaneous recovery after spinal cord injury and statistical power needed for therapeutic clinical trials. Spinal Cord *45*, 190–205. https://doi.org/10.1038/sj.sc.3102007.

7. Courtine, G., Roy, R.R., Raven, J., Hodgson, J., McKay, H., Yang, H., Zhong, H., Tuszynski, M.H., and Edgerton, V.R. (2005). Performance of locomotion and foot grasping following a unilateral thoracic corticospinal tract lesion in monkeys (Macaca mulatta). Brain. *128* (Pt 10), 2338–2358. https://doi.org/10.1093/brain/awh604.

8. Rosenzweig, E.S., Brock, J.H., Lu, P., Kumamaru, H., Salegio, E.A., Kadoya, K., Weber, J.L., Liang, J.J., Moseanko, R., Hawbecker, S., et al. (2018). Restorative effects of human neural stem cell grafts on the primate spinal cord. Nat. Med. *24*, 484–490. https://doi.org/10.1038/nm.4502.

9. Rosenzweig, E.S., Courtine, G., Jindrich, D.L., Brock, J.H., Ferguson, A.R., Strand, S.C., Nout, Y.S., Roy, R.R., Miller, D.M., Beattie, M.S., et al. (2010). Extensive spontaneous plasticity of corticospinal projections after primate spinal cord injury. Nat. Neurosci. *13*, 1505–1510. https://doi.org/10.1038/nn.2691.

10. Rosenzweig, E.S., Salegio, E.A., Liang, J.J., Weber, J.L., Weinholtz, C.A., Brock, J.H., Moseanko, R., Hawbecker, S., Pender, R., Cruzen, C.L., et al. (2019). Chondroitinase improves anatomical and functional outcomes after primate spinal cord injury. Nat. Neurosci. *22*, 1269–1275. https://doi.org/10.1038/s41593-019-0424-1.

11. Cao, Y., Shi, Y., Xiao, Z., Chen, X., Chen, B., Yang, B., Shu, M., Yin, Y., Wu, S., Yin, W., et al. (2021). Contralateral Axon Sprouting but Not Ipsilateral Regeneration Is Responsible for Spontaneous Locomotor Recovery Post Spinal Cord Hemisection. Front. Cell. Neurosci. *15*, 730348. https://doi.org/10.3389/fncel.2021.730348.

12. Ballermann, M., and Fouad, K. (2006). Spontaneous locomotor recovery in spinal cord injured rats is accompanied by anatomical plasticity of reticulospinal fibers. Eur. J. Neurosci. *23*, 1988–1996. https://doi.org/10.1111/j.1460-9568.2006.04726.x.

13. Courtine, G., Song, B., Roy, R.R., Zhong, H., Herrmann, J.E., Ao, Y., Qi, J., Edgerton, V.R., and Sofroniew, M.V. (2008). Recovery of supraspinal control of stepping via indirect propriospinal relay connections after spinal cord injury. Nat. Med. *14*, 69–74. https://doi.org/10.1038/nm1682.

14. Rowald, A., Komi, S., Demesmaeker, R., Baaklini, E., Hernandez-Charpak, S.D., Paoles, E., Montanaro, H., Cassara, A., Becce, F., Lloyd, B., et al. (2022). Activity-dependent spinal cord neuromodulation rapidly restores trunk and leg motor functions after complete paralysis. Nat. Med. *28*, 260–271. https://doi.org/10.1038/s41591-021-01663-5.

15. Jin, D., Liu, Y., Sun, F., Wang, X., Liu, X., and He, Z. (2015). Restoration of skilled locomotion by sprouting corticospinal axons induced by co-deletion of PTEN and SOCS3. Nat. Commun. *6*, 8074. https://doi.org/10.1038/ncomms9074.

16. Yokota, K., Kubota, K., Kobayakawa, K., Saito, T., Hara, M., Kijima, K., Maeda, T., Katoh, H., Ohkawa, Y., Nakashima, Y., and Okada, S. (2019). Pathological changes of distal motor neurons after complete spinal cord injury. Mol. Brain *12*, 4. https://doi.org/10.1186/s13041-018-0422-3.

17. Bertels, H., Vicente-Ortiz, G., El Kanbi, K., and Takeoka, A. (2022). Neurotransmitter phenotype switching by spinal excitatory interneurons regulates locomotor recovery after spinal cord injury. Nat. Neurosci. *25*, 617–629. https://doi.org/10.1038/s41593-022-01067-9.

18. Kim, D., Zai, L., Liang, P., Schaffling, C., Ahlborn, D., and Benowitz, L.I. (2013). Inosine enhances axon sprouting and motor recovery after spinal cord injury. PLoS One *8*, e81948. https://doi.org/10.1371/journal.pone.0081948.

19. Assinck, P., Duncan, G.J., Hilton, B.J., Plemel, J.R., and Tetzlaff, W. (2017). Cell transplantation therapy for spinal cord injury. Nat. Neurosci. *20*, 637–647. https://doi.org/10.1038/nn.4541.

20. Fischer, I., Dulin, J.N., and Lane, M.A. (2020). Transplanting neural progenitor cells to restore connectivity after spinal cord injury. Nat. Rev. Neurosci. *21*, 366–383. https://doi.org/10.1038/s41583-020-0314-2.

21. Ceto, S., Sekiguchi, K.J., Takashima, Y., Nimmerjahn, A., and Tuszynski, M.H. (2020). Neural Stem Cell Grafts Form Extensive Synaptic Networks that Integrate with Host Circuits after Spinal Cord Injury. Cell Stem Cell *27*, 430–440.e5. https://doi.org/10.1016/j.stem.2020.07.007.

22. Lepore, A.C., and Fischer, I. (2005). Lineage-restricted neural precursors survive, migrate, and differentiate following transplantation into the injured adult spinal cord. Exp. Neurol. *194*, 230–242. https://doi.org/10.1016/j.expneurol.2005.02.020.

23. Khazaei, M., Ahuja, C.S., Nakashima, H., Nagoshi, N., Li, L., Wang, J., Chio, J., Badner, A., Seligman, D., Ichise, A., et al. (2020). GDNF rescues the fate of neural progenitor grafts by attenuating Notch signals in the injured spinal cord in rodents. Sci. Transl. Med. *12*, eaau3538. https://doi.org/10.1126/scitranslmed.aau3538.

24. Bráz, J.M., Sharif-Naeini, R., Vogt, D., Kriegstein, A., Alvarez-Buylla, A., Rubenstein, J.L., and Basbaum, A.I. (2012). Forebrain GABAergic neuron precursors integrate into adult spinal cord and reduce injury-induced neuropathic pain. Neuron *74*, 663–675. https://doi.org/10.1016/j.neuron.2012.02.033.

25. Grumbles, R.M., Liu, Y., Thomas, C.M., Wood, P.M., and Thomas, C.K. (2013). Acute stimulation of transplanted neurons improves motoneuron survival, axon growth, and muscle reinnervation. J. Neurotrauma *30*, 1062–1069. https://doi.org/10.1089/neu.2012.2797.

26. Grade, S., and Götz, M. (2017). Neuronal replacement therapy: previous achievements and challenges ahead. NPJ Regen. Med. *2*, 29. https://doi.org/10.1038/s41536-017-0033-0.

27. Kjell, J., and Svensson, M. (2022). Advancing Peripheral Nerve Graft Transplantation for Incomplete Spinal Cord Injury Repair. Front. Cell. Neurosci. *16*, 885245. https://doi.org/10.3389/fncel.2022.885245.

28. Rosario, C.M., Aldskogius, H., Carlstedt, T., and Sidman, R.L. (1992). Centrifugal growth in orthotopic grafts of allogeneic dorsal root ganglia in adult rats: evidence for possible central ingrowth? Exp. Neurol. *115*, 158–162. https://doi.org/10.1016/0014-4886(92)90241-h.

29. Rosario, C.M., Aldskogius, H., Carlstedt, T., and Sidman, R.L. (1993). Differentiation and axonal outgrowth pattern of fetal dorsal root ganglion cells orthotopically allografted into adult rats. Exp. Neurol. *120*, 16–31. https://doi.org/10.1006/exnr.1993.1037.

30. Rosario, C.M., Dubovy, P., Sidman, R.L., and Aldskogius, H. (1995). Peripheral target reinnervation following orthotopic grafting of fetal allogeneic and xenogeneic dorsal root ganglia. Exp. Neurol. *132*, 251–261. https://doi.org/10.1016/0014-4886(95)90030-6.

31. Davies, S.J., Fitch, M.T., Memberg, S.P., Hall, A.K., Raisman, G., and Silver, J. (1997). Regeneration of adult axons in white matter tracts of the central nervous system. Nature *390*, 680–683. https://doi.org/10.1038/37776.

32. Davies, S.J., Goucher, D.R., Doller, C., and Silver, J. (1999). Robust regeneration of adult sensory axons in degenerating white matter of the adult rat spinal cord. J. Neurosci. *19*, 5810–5822. https://doi.org/10.1523/JNEUROSCI.19-14-05810.1999.

33. Pfisterer, U., and Khodosevich, K. (2017). Neuronal survival in the brain: neuron type-specific mechanisms. Cell Death Dis. *8*, e2643. https://doi.org/10.1038/cddis.2017.64.

34. Wong Fong Sang, I.E., Schroer, J., Halbhuber, L., Warm, D., Yang, J.W., Luhmann, H.J., Kilb, W., and Sinning, A. (2021). Optogenetically Controlled Activity Pattern Determines Survival Rate of Developing Neocortical Neurons. Int. J. Mol. Sci. *22*, 6575. https://doi.org/10.3390/ijms22126575.

35. Warm, D., Bassetti, D., Schroer, J., Luhmann, H.J., and Sinning, A. (2022). Spontaneous Activity Predicts Survival of Developing Cortical Neurons. Front. Cell Dev. Biol. *10*, 937761. https://doi.org/10.3389/fcell.2022.937761.

36. Xue, M., Atallah, B.V., and Scanziani, M. (2014). Equalizing excitation-inhibition ratios across visual cortical neurons. Nature *511*, 596–600. https://doi.org/10.1038/nature13321.

37. Kelsch, W., Lin, C.W., Mosley, C.P., and Lois, C. (2009). A critical period for activity-dependent synaptic development during olfactory bulb adult neurogenesis. J. Neurosci. *29*, 11852–11858. https://doi.org/10.1523/JNEUROSCI.2406-09.2009.

38. Priya, R., Paredes, M.F., Karayannis, T., Yusuf, N., Liu, X., Jaglin, X., Graef, I., Alvarez-Buylla, A., and Fishell, G. (2018). Activity Regulates Cell Death within Cortical Interneurons through a Calcineurin-Dependent Mechanism. Cell Rep. *22*, 1695–1709. https://doi.org/10.1016/j.celrep.2018.01.007.

39. Lin, C.W., Sim, S., Ainsworth, A., Okada, M., Kelsch, W., and Lois, C. (2010). Genetically increased cell-intrinsic excitability enhances neuronal integration into adult brain circuits. Neuron *65*, 32–39. https://doi.org/10.1016/j.neuron.2009.12.001.

40. Zhu, C., Jiang, Z., Xu, Y., Cai, Z.L., Jiang, Q., Xu, Y., Xue, M., Arenkiel, B.R., Wu, Q., Shu, G., and Tong, Q. (2020). Profound and redundant functions of arcuate neurons in obesity development. Nat. Metab. *2*, 763–774. https://doi.org/10.1038/s42255-020-0229-2.

41. Bando, Y., Irie, K., Shimomura, T., Umeshima, H., Kushida, Y., Kengaku, M., Fujiyoshi, Y., Hirano, T., and Tagawa, Y. (2016). Control of Spontaneous Ca2+ Transients Is Critical for Neuronal Maturation in the Developing Neocortex. Cereb. Cortex *26*, 106–117. https://doi.org/10.1093/cercor/bhu180.

42. Halls, M.L., and Cooper, D.M.F. (2011). Regulation by Ca2+-signaling pathways of adenylyl cyclases. Cold Spring Harb. Perspect. Biol. *3*, a004143. https://doi.org/10.1101/cshperspect.a004143.

43. Kourti, M., Liaropoulou, D., Paschou, M., Giagklisi, I., Paschalidi, M., Petani, E., and Papazafiri, P. (2022). Enhanced Ca(2+) Entry Sustains the Activation of Akt in Glucose Deprived SH-SY5Y Cells. Int. J. Mol. Sci. *23*, 1386. https://doi.org/10.3390/ijms23031386.

44. Hou, Y., Wang, K., Wan, W., Cheng, Y., Pu, X., and Ye, X. (2018). Resveratrol provides neuroprotection by regulating the JAK2/STAT3/PI3K/AKT/mTOR pathway after stroke in rats. Genes Dis. *5*, 245–255. https://doi.org/10.1016/j.gendis.2018.06.001.

45. Deng, H., Yue, J.K., Zusman, B.E., Nwachuku, E.L., Abou-Al-Shaar, H., Upadhyayula, P.S., Okonkwo, D.O., and Puccio, A.M. (2020). B-Cell Lymphoma 2 (Bcl-2) and Regulation of Apoptosis after Traumatic Brain Injury: A Clinical Perspective. Medicina (Kaunas) *56*, 300. https://doi.org/10.3390/medicina56060300.

46. Pemberton, J.M., Pogmore, J.P., and Andrews, D.W. (2021). Neuronal cell life, death, and axonal degeneration as regulated by the BCL-2 family proteins. Cell Death Differ. *28*, 108–122. https://doi.org/10.1038/s41418-020-00654-2.

47. Deogracias, R., Espliguero, G., Iglesias, T., and Rodríguez-Peña, A. (2004). Expression of the neurotrophin receptor trkB is regulated by the cAMP/CREB pathway in neurons. Mol. Cell. Neurosci. *26*, 470–480. https://doi.org/10.1016/j.mcn.2004.03.007.

48. Fearnley, G.W., Bruns, A.F., Wheatcroft, S.B., and Ponnambalam, S. (2015). VEGF-A isoform-specific regulation of calcium ion flux, transcriptional activation and endothelial cell migration. Biol. Open *4*, 731–742. https://doi.org/10.1242/bio.201410884.

49. Pérez-García, M.J., Ceña, V., de Pablo, Y., Llovera, M., Comella, J.X., and Soler, R.M. (2004). Glial cell line-derived neurotrophic factor increases intracellular calcium concentration. Role of calcium/calmodulin in the activation of the phosphatidylinositol 3-kinase pathway. J. Biol. Chem. *279*, 6132–6142. https://doi.org/10.1074/jbc.M308367200.

50. Hilton, B.J., Blanquie, O., Tedeschi, A., and Bradke, F. (2019). High-resolution 3D imaging and analysis of axon regeneration in unsectioned spinal cord with or without tissue clearing. Nat. Protoc. *14*, 1235–1260. https://doi.org/10.1038/s41596-019-0140-z.

51. Usoskin, D., Furlan, A., Islam, S., Abdo, H., Lönnerberg, P., Lou, D., Hjerling-Leffler, J., Haeggström, J., Kharchenko, O., Kharchenko, P.V., et al. (2015). Unbiased classification of sensory neuron types by large-scale single-cell RNA sequencing. Nat. Neurosci. *18*, 145–153. https://doi.org/10.1038/nn.3881.

52. Zheng, Y., Liu, P., Bai, L., Trimmer, J.S., Bean, B.P., and Ginty, D.D. (2019). Deep Sequencing of Somatosensory Neurons Reveals Molecular Determinants of Intrinsic Physiological Properties. Neuron *103*, 598–616.e7. https://doi.org/10.1016/j.neuron.2019.05.039.

53. Li, K., Figarella, K., Su, X., Kovalchuk, Y., Gorzolka, J., Neher, J.J., Mojtahedi, N., Casadei, N., Hedrich, U.B.S., and Garaschuk, O. (2023). Endogenous but not sensory-driven activity controls migration, morphogenesis and survival of adult-born juxtaglomerular neurons in the mouse olfactory bulb. Cell. Mol. Life Sci. *80*, 98. https://doi.org/10.1007/s00018-023-04753-4.

54. Piltti, K.M., Avakian, S.N., Funes, G.M., Hu, A., Uchida, N., Anderson, A.J., and Cummings, B.J. (2015). Transplantation dose alters the dynamics of human neural stem cell engraftment, proliferation and migration after spinal cord injury. Stem Cell Res. *15*, 341–353. https://doi.org/10.1016/j.scr.2015.07.001.

55. Poplawski, G.H., and Tuszynski, M.H. (2020). Regeneration of Corticospinal Axons into Neural Progenitor Cell Grafts After Spinal Cord Injury. Neurosci. Insights *15*, 2633105520974000. https://doi.org/10.1177/2633105520974000.

56. Carmichael, S.T., and Chesselet, M.F. (2002). Synchronous neuronal activity is a signal for axonal sprouting after cortical lesions in the adult. J. Neurosci. *22*, 6062–6070. https://doi.org/10.1523/JNEUROSCI.22-14-06062.2002.

57. Zareen, N., Dodson, S., Armada, K., Awad, R., Sultana, N., Hara, E., Alexander, H., and Martin, J.H. (2018). Stimulation-dependent remodeling of the corticospinal tract requires reactivation of growth-promoting developmental signaling pathways. Exp. Neurol. *307*, 133–144. https://doi.org/10.1016/j.expneurol.2018.05.004.

58. Fouad, K., Rank, M.M., Vavrek, R., Murray, K.C., Sanelli, L., and Bennett, D.J. (2010). Locomotion after spinal cord injury depends on constitutive activity in serotonin receptors. J. Neurophysiol. *104*, 2975–2984. https://doi.org/10.1152/jn.00499.2010.

59. Basso, D.M., Fisher, L.C., Anderson, A.J., Jakeman, L.B., McTigue, D.M., and Popovich, P.G. (2006). Basso Mouse Scale for locomotion detects differences in recovery after spinal cord injury in five common mouse strains. J. Neurotrauma *23*, 635–659. https://doi.org/10.1089/neu.2006.23.635.

60. Cummings, B.J., Engesser-Cesar, C., Cadena, G., and Anderson, A.J. (2007). Adaptation of a ladder beam walking task to assess locomotor recovery in mice following spinal cord injury. Behav. Brain Res. *177*, 232–241. https://doi.org/10.1016/j.bbr.2006.11.042.

61. Bonilla, P., Hernandez, J., Giraldo, E., González-Pérez, M.A., Alastrue-Agudo, A., Elkhenany, H., Vicent, M.J., Navarro, X., Edel, M., and Moreno-Manzano, V. (2021). Human-Induced Neural and Mesenchymal Stem Cell Therapy Combined with a Curcumin Nanoconjugate as a Spinal Cord Injury Treatment. Int. J. Mol. Sci. *22*, 5966. https://doi.org/10.3390/ijms22115966.

62. Fouad, K., Pedersen, V., Schwab, M.E., and Brösamle, C. (2001). Cervical sprouting of corticospinal fibers after thoracic spinal cord injury accompanies shifts in evoked motor responses. Curr. Biol. *11*, 1766–1770. https://doi.org/10.1016/s0960-9822(01)00535-8.

63. Onifer, S.M., Smith, G.M., and Fouad, K. (2011). Plasticity after spinal cord injury: relevance to recovery and approaches to facilitate it. Neurotherapeutics *8*, 283–293. https://doi.org/10.1007/s13311-011-0034-4.

64. Bhowmick, S., and Abdul-Muneer, P.M. (2021). PTEN Blocking Stimulates Corticospinal and Raphespinal Axonal Regeneration and Promotes Functional Recovery After Spinal Cord Injury. J. Neuropathol. Exp. Neurol. *80*, 169–181. https://doi.org/10.1093/jnen/nlaa147.

65. Alvarez, F.J., Villalba, R.M., Zerda, R., and Schneider, S.P. (2004). Vesicular glutamate transporters in the spinal cord, with special reference to sensory primary afferent synapses. J. Comp. Neurol. *472*, 257–280. https://doi.org/10.1002/cne.20012.

66. Du Beau, A., Shakya Shrestha, S., Bannatyne, B.A., Jalicy, S.M., Linnen, S., and Maxwell, D.J. (2012). Neurotransmitter phenotypes of descending systems in the rat lumbar spinal cord. Neuroscience *227*, 67–79. https://doi.org/10.1016/j.neuroscience.2012.09.037.

67. Chaudhry, F.A., Reimer, R.J., Bellocchio, E.E., Danbolt, N.C., Osen, K.K., Edwards, R.H., and Storm-Mathisen, J. (1998). The vesicular GABA transporter, VGAT, localizes to synaptic vesicles in sets of glycinergic as well as GABAergic neurons. J. Neurosci. *18*, 9733–9750. https://doi.org/10.1523/JNEUROSCI.18-23-09733.1998.

68. Beauparlant, J., van den Brand, R., Barraud, Q., Friedli, L., Musienko, P., Dietz, V., and Courtine, G. (2013). Undirected compensatory plasticity contributes to neuronal dysfunction after severe spinal cord injury. Brain. *136* (Pt 11), 3347–3361. https://doi.org/10.1093/brain/awt204.

69. Brini, M., Calì, T., Ottolini, D., and Carafoli, E. (2014). Neuronal calcium signaling: function and dysfunction. Cell. Mol. Life Sci. *71*, 2787–2814. https://doi.org/10.1007/s00018-013-1550-7.

70. Cameron, E.G., and Kapiloff, M.S. (2017). Intracellular compartmentation of cAMP promotes neuroprotection and regeneration of CNS neurons. Neural Regen. Res. *12*, 201–202. https://doi.org/10.4103/1673-5374.200797.

71. Inglebert, Y., and Debanne, D. (2021). Calcium and Spike Timing-Dependent Plasticity. Front. Cell. Neurosci. *15*, 727336. https://doi.org/10.3389/fncel.2021.727336.

72. Shahoha, M., Cohen, R., Ben-Simon, Y., and Ashery, U. (2022). cAMP-Dependent Synaptic Plasticity at the Hippocampal Mossy Fiber Terminal. Front. Synaptic Neurosci. *14*, 861215. https://doi.org/10.3389/fnsyn.2022.861215.

73. Neumann, S., and Woolf, C.J. (1999). Regeneration of dorsal column fibers into and beyond the lesion site following adult spinal cord injury. Neuron *23*, 83–91. https://doi.org/10.1016/s0896-6273(00)80755-2.

74. Neumann, S., Bradke, F., Tessier-Lavigne, M., and Basbaum, A.I. (2002). Regeneration of sensory axons within the injured spinal cord induced by intraganglionic cAMP elevation. Neuron *34*, 885–893. https://doi.org/10.1016/s0896-6273(02)00702-x.

75. Pearse, D.D., Pereira, F.C., Marcillo, A.E., Bates, M.L., Berrocal, Y.A., Filbin, M.T., and Bunge, M.B. (2004). cAMP and Schwann cells promote axonal growth and functional recovery after spinal cord injury. Nat. Med. *10*, 610–616. https://doi.org/10.1038/nm1056.

76. Qiu, J., Cai, D., Dai, H., McAtee, M., Hoffman, P.N., Bregman, B.S., and Filbin, M.T. (2002). Spinal axon regeneration induced by elevation of cyclic AMP. Neuron *34*, 895–903. https://doi.org/10.1016/s0896-6273(02)00730-4.

77. Bonneau, B., Prudent, J., Popgeorgiev, N., and Gillet, G. (2013). Non-apoptotic roles of Bcl-2 family: the calcium connection. Biochim. Biophys. Acta *1833*, 1755–1765. https://doi.org/10.1016/j.bbamcr.2013.01.021.

78. Amemiya, Y., Maki, M., Shibata, H., and Takahara, T. (2023). New Insights into the Regulation of mTOR Signaling via Ca(2+)-Binding Proteins. Int. J. Mol. Sci. *24*, 3923. https://doi.org/10.3390/ijms24043923.

79. Duan, X., Qiao, M., Bei, F., Kim, I.J., He, Z., and Sanes, J.R. (2015). Subtype-specific regeneration of retinal ganglion cells following axotomy: effects of osteopontin and mTOR signaling. Neuron *85*, 1244–1256. https://doi.org/10.1016/j.neuron.2015.02.017.

80. Chen, N., Zhou, P., Liu, X., Li, J., Wan, Y., Liu, S., and Wei, F. (2020). Overexpression of Rictor in the injured spinal cord promotes functional recovery in a rat model of spinal cord injury. FASEB J. *34*, 6984–6998. https://doi.org/10.1096/fj.201903171R.

81. Harvey, A.R., Lovett, S.J., Majda, B.T., Yoon, J.H., Wheeler, L.P.G., and Hodgetts, S.I. (2015). Neurotrophic factors for spinal cord repair: Which, where, how and when to apply, and for what period of time? Brain Res. *1619*, 36–71. https://doi.org/10.1016/j.brainres.2014.10.049.

82. Weishaupt, N., Blesch, A., and Fouad, K. (2012). BDNF: the career of a multifaceted neurotrophin in spinal cord injury. Exp. Neurol. *238*, 254–264. https://doi.org/10.1016/j.expneurol.2012.09.001.

83. Wang, L., Gu, S., Gan, J., Tian, Y., Zhang, F., Zhao, H., and Lei, D. (2021). Neural Stem Cells Overexpressing Nerve Growth Factor Improve Functional Recovery in Rats Following Spinal Cord Injury via Modulating Microenvironment and Enhancing Endogenous Neurogenesis. Front. Cell. Neurosci. *15*, 773375. https://doi.org/10.3389/fncel.2021.773375.

84. Widenfalk, J., Lipson, A., Jubran, M., Hofstetter, C., Ebendal, T., Cao, Y., and Olson, L. (2003). Vascular endothelial growth factor improves functional outcome and decreases secondary degeneration in experimental spinal cord contusion injury. Neuroscience *120*, 951–960. https://doi.org/10.1016/s0306-4522(03)00399-3.

85. Ortmann, S.D., and Hellenbrand, D.J. (2018). Glial cell line-derived neurotrophic factor as a treatment after spinal cord injury. Neural Regen. Res. *13*, 1733–1734. https://doi.org/10.4103/1673-5374.238610.

86. Zhang, D., Yuan, Y., Zhu, J., Zhu, D., Li, C., Cui, W., Wang, L., Ma, S., Duan, S., and Liu, B. (2021). Insulin-like growth factor 1 promotes neurological functional recovery after spinal cord injury through inhibition of autophagy via the PI3K/Akt/mTOR signaling pathway. Exp. Ther. Med. *22*, 1265. https://doi.org/10.3892/etm.2021.10700.

87. Huang, X., Kim, J.M., Kong, T.H., Park, S.R., Ha, Y., Kim, M.H., Park, H., Yoon, S.H., Park, H.C., Park, J.O., et al. (2009). GM-CSF inhibits glial scar formation and shows long-term protective effect after spinal cord injury. J. Neurol. Sci. *277*, 87–97. https://doi.org/10.1016/j.jns.2008.10.022.

88. Guo, X.Y., Duan, F.X., Chen, J., Wang, Y., Wang, R., Shen, L., Qi, Q., Jiang, Z.Q., Zhu, A.Y., Xi, J., et al. (2019). Subcutaneous Administration of PDGF-AA Improves the Functional Recovery After Spinal Cord Injury. Front. Neurosci. *13*, 6. https://doi.org/10.3389/fnins.2019.00006.

89. Spitzer, N.C. (2006). Electrical activity in early neuronal development. Nature *444*, 707–712. https://doi.org/10.1038/nature05300.

90. Itoh, K., Ozaki, M., Stevens, B., and Fields, R.D. (1997). Activity-dependent regulation of N-cadherin in DRG neurons: Differential regulation of N-cadherin, NCAM, and L1 by distinct patterns of action potentials. J. Neurobiol. *33*, 735–748. https://doi.org/10.1002/(sici)1097-4695(19971120)33:6<735::Aid-neu3>3.0.Co;2-a.

91. van den Brand, R., Heutschi, J., Barraud, Q., DiGiovanna, J., Bartholdi, K., Huerlimann, M., Friedli, L., Vollenweider, I., Moraud, E.M., Duis, S., et al. (2012). Restoring voluntary control of locomotion after paralyzing spinal cord injury. Science *336*, 1182–1185. https://doi.org/10.1126/science.1217416.

92. Faust, T.E., Gunner, G., and Schafer, D.P. (2021). Mechanisms governing activity-dependent synaptic pruning in the developing mammalian CNS. Nat. Rev. Neurosci. *22*, 657–673. https://doi.org/10.1038/s41583-021-00507-y.

93. Girgis, J., Merrett, D., Kirkland, S., Metz, G.A.S., Verge, V., and Fouad, K. (2007). Reaching training in rats with spinal cord injury promotes plasticity and task specific recovery. Brain. *130* (Pt 11), 2993–3003. https://doi.org/10.1093/brain/awm245.

94. Goldshmit, Y., Lythgo, N., Galea, M.P., and Turnley, A.M. (2008). Treadmill training after spinal cord hemisection in mice promotes axonal sprouting and synapse formation and improves motor recovery. J. Neurotrauma *25*, 449–465. https://doi.org/10.1089/neu.2007.0392.

95. Fouad, K., and Tetzlaff, W. (2012). Rehabilitative training and plasticity following spinal cord injury. Exp. Neurol. *235*, 91–99. https://doi.org/10.1016/j.expneurol.2011.02.009.

96. Tikhonov, D.B., and Zhorov, B.S. (2005). Sodium channel activators: model of binding inside the pore and a possible mechanism of action. FEBS Lett. *579*, 4207–4212. https://doi.org/10.1016/j.febslet.2005.07.017.

97. Gao, X., Hu, J., Zhang, X., Zuo, Y., Wang, Y., and Zhu, S. (2020). Research progress of aconitine toxicity and forensic analysis of aconitine poisoning. Forensic Sci. Res. *5*, 25–31. https://doi.org/10.1080/20961790.2018.1452346.

98. Jang, E.H., Sim, A., Im, S.K., and Hur, E.M. (2016). Effects of Microtubule Stabilization by Epothilone B Depend on the Type and Age of Neurons. Neural Plast. *2016*, 5056418. https://doi.org/10.1155/2016/5056418.

99. Ding, B., and Kilpatrick, D.L. (2013). Lentiviral vector production, titration, and transduction of primary neurons. Methods Mol. Biol. *1018*, 119–131. https://doi.org/10.1007/978-1-62703-444-9_12.

100. Sánchez-Huertas, C., Freixo, F., Viais, R., Lacasa, C., Soriano, E., and Lüders, J. (2016). Non-centrosomal nucleation mediated by augmin organizes microtubules in post-mitotic neurons and controls axonal microtubule polarity. Nat. Commun. *7*, 12187. https://doi.org/10.1038/ncomms12187.

101. Rubinson, D.A., Dillon, C.P., Kwiatkowski, A.V., Sievers, C., Yang, L., Kopinja, J., Rooney, D.L., Zhang, M., Ihrig, M.M., McManus, M.T., et al. (2003). A lentivirus-based system to functionally silence genes in primary mammalian cells, stem cells and transgenic mice by RNA interference. Nat. Genet. *33*, 401–406. https://doi.org/10.1038/ng1117.

102. Monreal-Trigo, J., Terres-Haro, J.M., Martinez-Rojas, B., Sanchez-Martin, M.D.M., Giraldo, E., Moreno Manzano, V., and Alcaniz Fillol, M. (2022). Optogenetic Stimulation Array for Confocal Microscopy Fast Transient Monitoring. IEEE Trans. Biomed. Circuits Syst. *16*, 1397–1405. https://doi.org/10.1109/TBCAS.2022.3226558.

103. Virtanen, S.S., Kukkonen-Macchi, A., Vainio, M., Elima, K., Härkönen, P.L., Jalkanen, S., and Yegutkin, G.G. (2014). Adenosine inhibits tumor cell invasion via receptor-independent mechanisms. Mol. Cancer Res. *12*, 1863–1874. https://doi.org/10.1158/1541-7786.MCR-14-0302-T.

104. Wojnicz, A., Avendaño-Ortiz, J., de Pascual, R., Ruiz-Pascual, L., García, A.G., and Ruiz-Nuño, A. (2016). Simultaneous monitoring of monoamines, amino acids, nucleotides and neuropeptides by liquid chromatography-tandem mass spectrometry and its application to neurosecretion in bovine chromaffin cells. J. Mass Spectrom. *51*, 651–664. https://doi.org/10.1002/jms.3794.

105. Lilley, E., Andrews, M.R., Bradbury, E.J., Elliott, H., Hawkins, P., Ichiyama, R.M., Keeley, J., Michael-Titus, A.T., Moon, L.D.F., Pluchino, S., et al. (2020). Refining rodent models of spinal cord injury. Exp. Neurol. *328*, 113273. https://doi.org/10.1016/j.expneurol.2020.113273.

106. Kathe, C., Skinnider, M.A., Hutson, T.H., Regazzi, N., Gautier, M., Demesmaeker, R., Komi, S., Ceto, S., James, N.D., Cho, N., et al. (2022). The neurons that restore walking after paralysis. Nature *611*, 540–547. https://doi.org/10.1038/s41586-022-05385-7.

107. Metz, G.A., and Whishaw, I.Q. (2002). Cortical and subcortical lesions impair skilled walking in the ladder rung walking test: a new task to evaluate fore- and hindlimb stepping, placing, and co-ordination. J. Neurosci. Methods *115*, 169–179. https://doi.org/10.1016/s0165-0270(02)00012-2.

108. Deuis, J.R., Dvorakova, L.S., and Vetter, I. (2017). Methods Used to Evaluate Pain Behaviors in Rodents. Front. Mol. Neurosci. *10*, 284. https://doi.org/10.3389/fnmol.2017.00284.

109. Tainaka, K., Murakami, T.C., Susaki, E.A., Shimizu, C., Saito, R., Takahashi, K., Hayashi-Takagi, A., Sekiya, H., Arima, Y., Nojima, S., et al. (2018). Chemical Landscape for Tissue Clearing Based on Hydrophilic Reagents. Cell Rep. *24*, 2196–2210.e9. https://doi.org/10.1016/j.celrep.2018.07.056.

110. Bradbury, E.J., and Burnside, E.R. (2019). Moving beyond the glial scar for spinal cord repair. Nat. Commun. *10*, 3879. https://doi.org/10.1038/s41467-019-11707-7.

111. Xia, L., Qi, J., Tang, M., Liu, J., Zhang, D., Zhu, Y., and Hu, B. (2022). Continual Deletion of Spinal Microglia Reforms Astrocyte Scar Favoring Axonal Regeneration. Front. Pharmacol. *13*, 881195. https://doi.org/10.3389/fphar.2022.881195.

112. Martínez-Rojas, B., Giraldo, E., Grillo-Risco, R., Hidalgo, M.R., López-Mocholi, E., Alastrue-Agudo, A., García-García, F., and Moreno-Manzano, V. (2022). NPC transplantation rescues sci-driven cAMP/EPAC2 alterations, leading to neuroprotection and microglial modulation. Cell. Mol. Life Sci. *79*, 455. https://doi.org/10.1007/s00018-022-04494-w.

113. Schaal, S.M., Garg, M.S., Ghosh, M., Lovera, L., Lopez, M., Patel, M., Louro, J., Patel, S., Tuesta, L., Chan, W.M., and Pearse, D.D. (2012). The therapeutic profile of rolipram, PDE target and mechanism of action as a neuroprotectant following spinal cord injury. PLoS One *7*, e43634. https://doi.org/10.1371/journal.pone.0043634.

YMTHE, Volume *32*

Supplemental Information

Transplantation of dorsal root ganglia overexpressing the NaChBac sodium channel improves locomotion after complete SCI

Sonia Hingorani, Guillem Paniagua Soriano, Carlos Sánchez Huertas, Eva María Villalba Riquelme, Eric López Mocholi, Beatriz Martínez Rojas, Ana Alastrué Agudo, Sebastián Dupraz, Antonio Vicente Ferrer Montiel, and Victoria Moreno Manzano

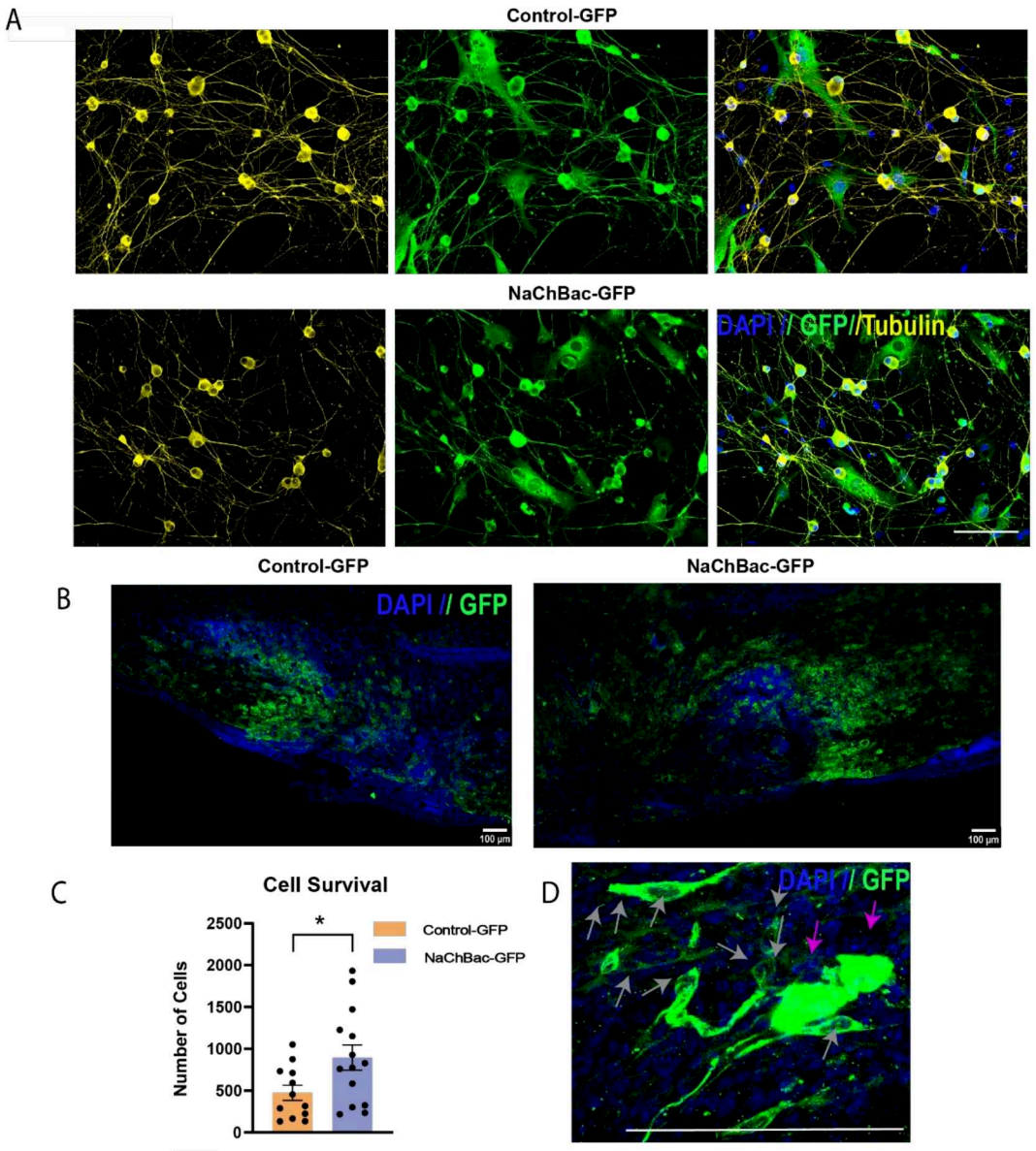

Figure S1. A) Images of infected dissociated DRG cultures expressing Control-GFP and NaChBac-GFP before transplantation. Green (GFP), yellow (β-III tubulin), blue (DAPI). Scale bar = 100 µm. **B)** Representative images of transplanted cells (green) fourteen days after lesion and transplantation, and **C)** Quantification of cell number**.** Unpaired t-test, p= 0.047; n=7-8. DAPI = Blue. Scale bar = 100 µm. **D)** Magnified images of glial cells (grey arrows) and neurons (magenta arrows) after transplantation. Note the difference in morphology and GFP expression. Data presented as mean ± SEM.

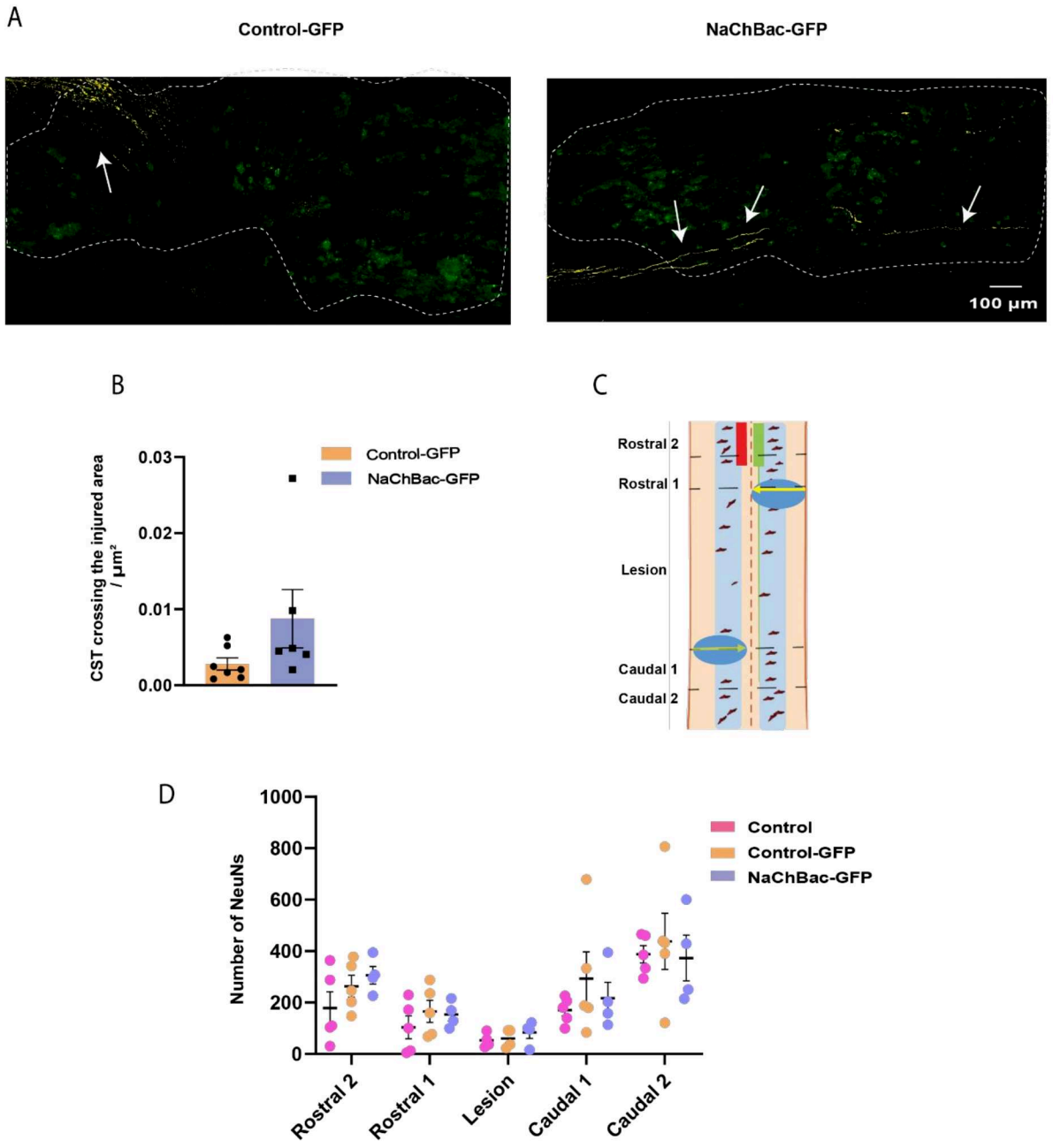

Figure S2. A) Representative images of the CST (yellow arrows) passing through transplanted cells (green). **B)** Quantification of the area of the CST passing through the transplant area. Unpaired T-test, p=0.16, n=7. **C)** Representation spinal cord division to quantify NeuN. **D)** Graph showing quantified NeuN, n=4-6, Two-way ANOVA followed by Tukey´s post hoc test. Data presented as mean ± SEM.

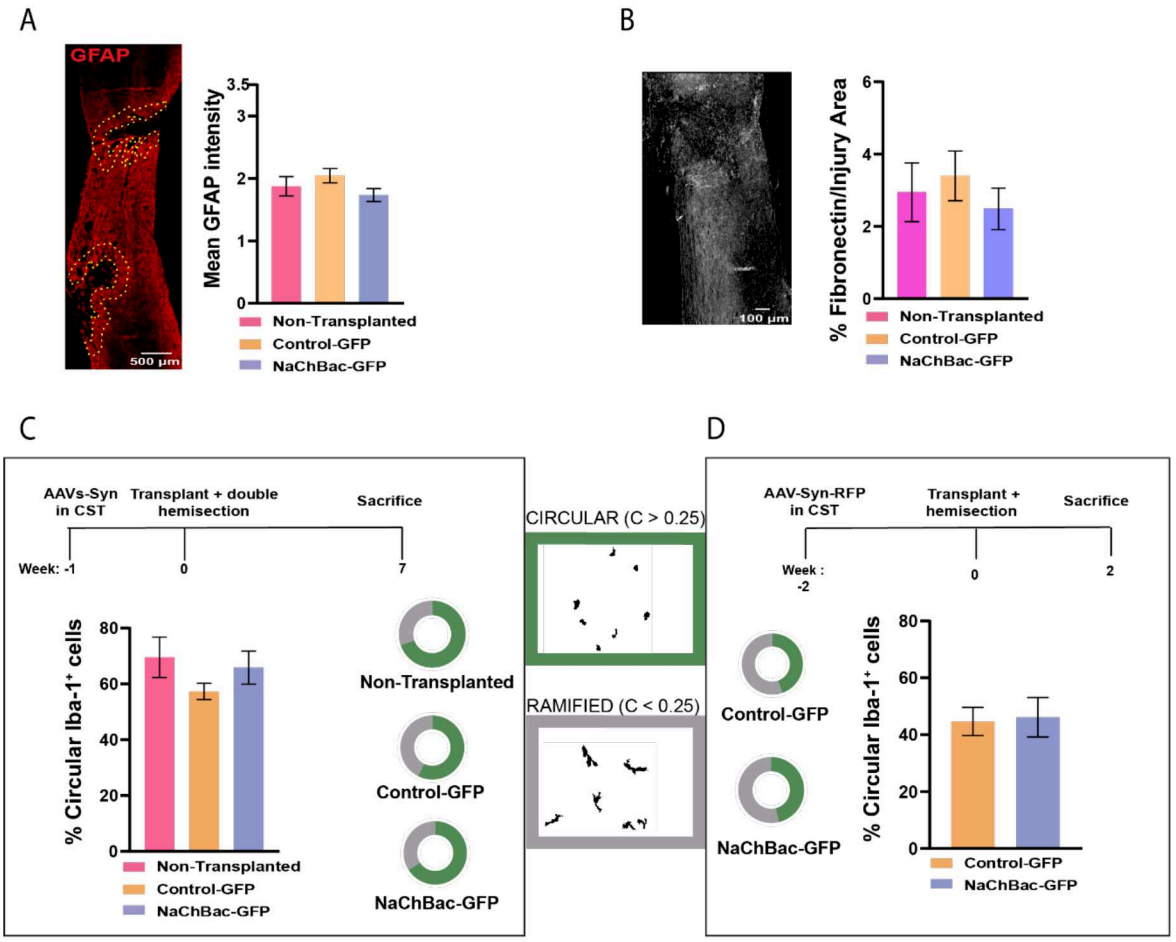

Figure S3. A) (Left) Representative images of border (yellow line) surrounding the injury, which is GFAP (red) negative. (Right) Graphical representation of the mean intensity of the border delimiting the injury in Non-Transplanted, Control-GFP and NaChBac-GFP animals. **B)** (Left)Representative image of fibronectin within the injury site between the two hemisections and graphical representation of fibronectin positive area within injury (left) in all three groups. **C)** (Top) Experimental timeline of the experiment analyzed, and graphical representation of % circular Iba-1 positive cells surrounding the injury in Non-Transplanted, Control-GFP and NaChBac-GFP mice (lower left). Depiction of mean % of circular and ramified microglia in all three groups (lower right). **D)** (Top) Experimental timeline of the experiment analyzed. (Lower left) Graphical representation of % circular Iba-1 positive cells surrounding the injury in Control-GFP and NaChBac-GFP mice. Depiction of mean % of circular and ramified microglia in all three groups (lower right).

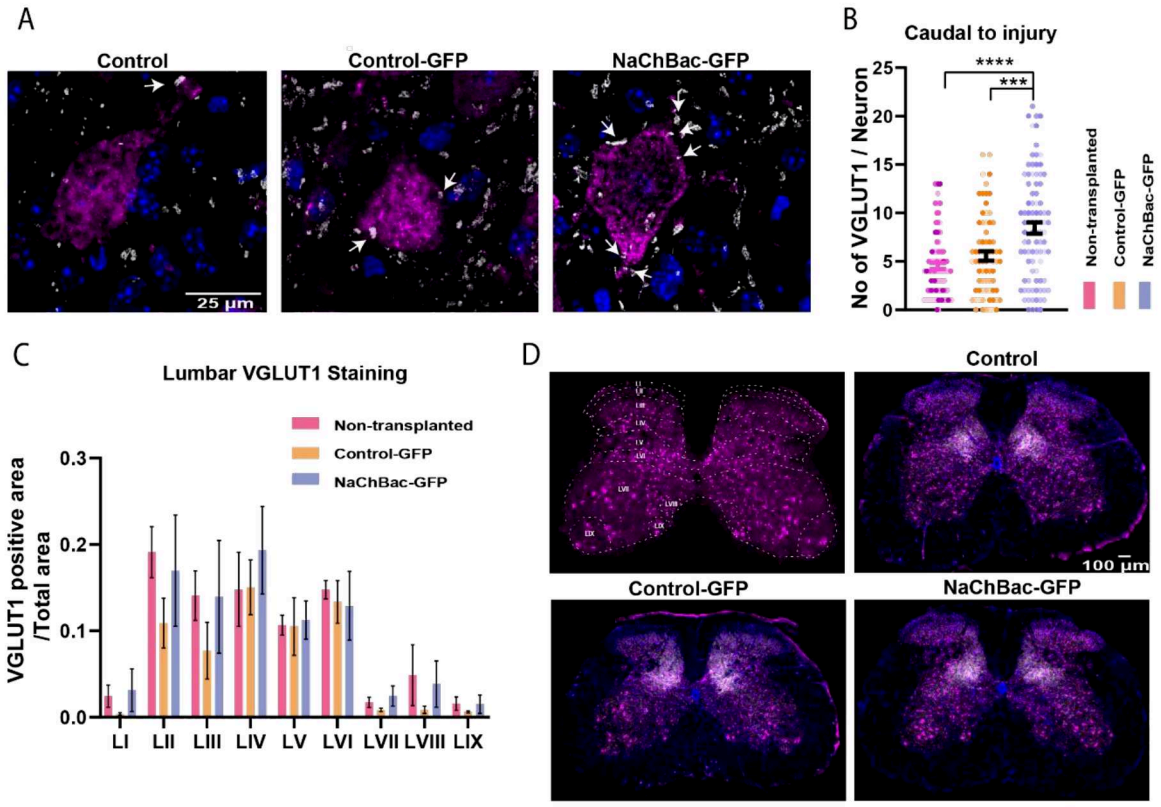

Figure S4. A) Images illustrating NeuN (magenta) in the Caudal 1 and 2 areas and VGlut1 (gray) contacting neurons. Arrows depict VGlut1 in contact with neurons. DAPI = blue; Scale bar = 25 µm. **B)** Quantification of VGLUT1 contacts per neuron. One-way ANOVA, Tukey´s post-test. **** Non Transplanted vs. NaChBac-GFP, p=0.0002; ***Control-GFP vs. NaChBac-GFP, p<0.0001. **C)** VGLUT1-positive area relative to total area quantified in the lumbar region of the spinal cord (L1-L6) **D)** Images showing the identified layers of VGlut1 staining in the lumbar spinal cord; NeuN (magenta), VGLUT1 (gray), DAPI (blue). Scale bar = 100 µm. Data presented as mean ± SEM.

Table S1. Additional electrophysiological parameters measured in Control-GFP and NaChBac-GFP DRG neurons. Input resistance (R_{input}), time to AP peak (t_{peak}), AP voltage threshold (Vth), repolarization time (tr), and after hyperpolarization amplitude (AHP). Data are shown as median (Q25-Q75). *Mann-Whitney test ***p=0.0002.*

	Control-GFP	**NaChBac-GFP**
Capacitance (pF)	16 (12-21)	17 (14-22)
R_{input} (MΩ)	416 (255-648)	447 (327-594)
t_{peak} (ms)	11 (9-13)	12 (9-15)
Vth (mV)	-21 (-23-(-16))	-17 (-23-(-15))
Overshoot (mV)	41 (22-48)	38 (29-48)
Amplitude (mV)	91 (73-100)	93 (77-102)
tr (ms)	4 (2-5)	4 (2-8)
AHP (mV)	17 (14-19)	10 (6-14) ***